Prolonged multi-phase magmatism due to plume lithosphere interaction as applied to the High Arctic Large Igneous Province

Björn H. Heyn[1], Grace E. Shephard[1,2], Clinton P. Conrad[1]

[1]Centre for Planetary Habitability, Department of Geosciences, University of Oslo, Norway
[2]Research School of Earth Sciences, Australian National University, Australia

Key Points:

- Mantle plumes interacting with changes in lithosphere thickness at craton edges can cause prolonged melting with pulses in the same region
- Rejuvenated melting happens underneath previously melt-affected thinned lithosphere several hundred km downstream of the plume stem
- The timing and duration of rejuvenated melting in models correspond to and therefore may explain observations of magmatic pulses from HALIP

Corresponding author: Björn H. Heyn, b.h.heyn@geo.uio.no

Abstract

The widespread High Arctic Large Igneous Province (HALIP) exhibits prolonged melting over more than 50 Myr, an observation that is difficult to reconcile with the classic view of large igneous provinces and associated melting in plume heads. Hence, the suggested plume-related origin and classification of HALIP as a large igneous province have been questioned. Here, we use numerical models that include melting and melt migration to investigate a rising plume interacting with variable lithosphere thickness, i.e. an extended-basin-to-craton setting. Models reveal significant spatial and temporal variations in melt volumes and pulses of melt production, including protracted melting for at least about 30-40 Myr, but only if migrating melt transports heat upwards and enhances local lithospheric thinning. Plume material deflected from underneath the Greenland craton can then re-activate melting zones below the previously plume-influenced Sverdrup Basin, even though the plume is already ∼500 km away. Hence, melting zones may not represent the location of the deeper plume stem at a given time. Plume flux pulses associated with mantle processes or magma processes within the crust may alter the timing and volume of secondary pulses and their surface expression. Our models suggest that HALIP magmatism is expected to exhibit plume-related trace element signatures throughout time, but potentially shift from mostly tholeiitic magmas in the first pulse towards more alkalic compositions for secondary pulses, with regional variations in timing of magma types. We propose that the prolonged period of rejuvenated magmatism of HALIP is consistent with plume impingement on a cratonic edge.

Plain Language Summary

Typically, large mantle upwellings ("mantle plumes") are expected to cause catastrophic large-scale but short-lived (within a few million years) volcanism. However, a massive past volcanic event now distributed onshore and offshore across the Arctic (the High Arctic Large Igneous Province - HALIP) defies this expectation. This wide-spread magmatism exhibits dates spanning more than 50 Myrs, with several pulses of increased activity. Based on this prolonged magmatism, it has been questioned whether all of it can be attributed to a mantle plume, despite the geochemistry of basalts indicating a plume source. Here, we show that a plume can cause prolonged melting including pulses of magmatism if it interacts with an increase in lithosphere thickness. Once the plume moved below the thicker lithosphere, hot plume material is channeled along the base of the lithosphere towards the adjacent thinner part, where it can reactivate previous melting regions. At this time, the active plume can be about 500 km away from the melting region, hence plume-related melt cannot be used as a proxy for the plume position at the given time. Based on the models, we suggest that the prolonged HALIP magmatism was caused by a plume impinging on the edge of a craton.

1 Introduction

Located at the geographic top of the world, the High Arctic Large Igneous Province (HALIP; (Tarduno, 1998; Maher, 2001)) is one of the most enigmatic volcanic provinces on Earth. Broadly speaking, HALIP is attributed to a range of Cretaceous aged (∼130-80 Ma) volcanic and magmatic rocks, currently distributed onshore and offshore around the circum-Arctic. HALIP includes flood basalts (both continental and oceanic), plutonic complexes, dykes, sills, and pyroclastic flows. They are dominantly tholeiitic in nature, but with numerous alkaline suites (e.g., Estrada et al., 2016). From roughly east to west, localities include the Canadian Arctic Islands, northern Greenland, the central Arctic Ocean (Alpha-Mendeleev Ridge), Svalbard, the Barents Shelf, Franz Josef Land, the De Long Islands, and Siberian shelves (Figure 1). The large geographic footprint of both intrusive and extrusive rocks is partly attributed to the mechanism of emplacement (i.e. mantle plume arrival) as well as subsequent dispersal via post-emplacement tectonic

motions (i.e. opening of the Eurasia Basin and Eurekan deformation). HALIP is also linked to significant regional oceanographic and climatic environmental changes (e.g., Galloway et al., 2022).

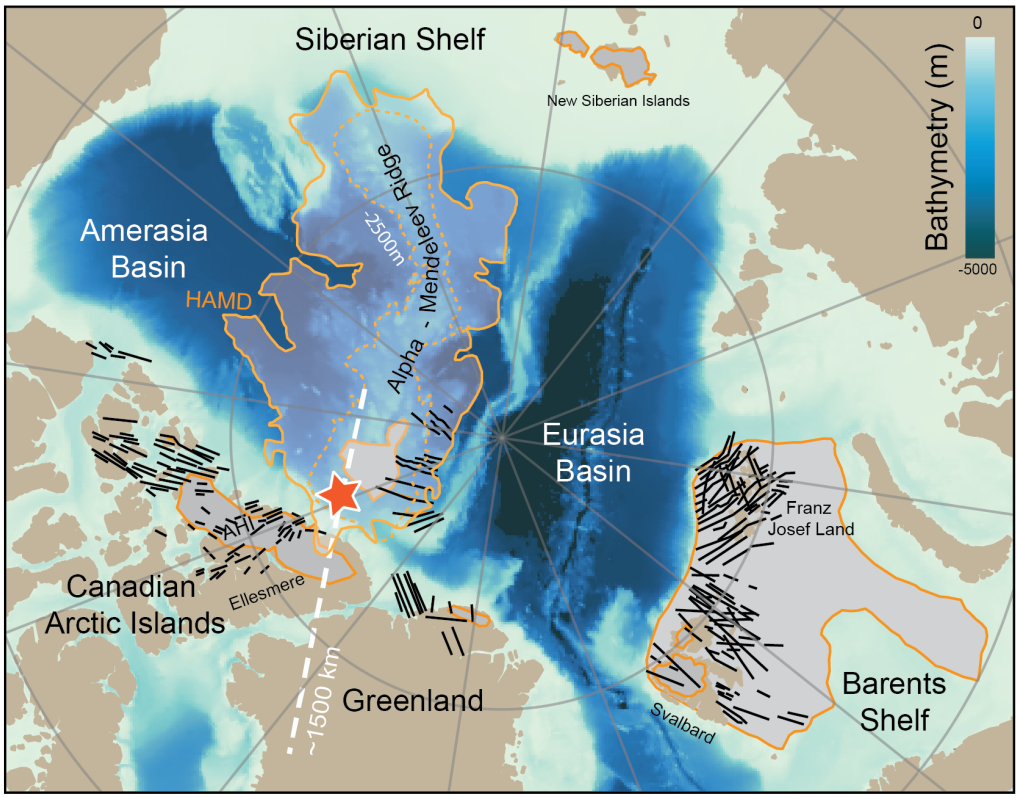

Figure 1: Overview of the Arctic domain at present-day (bathymetry - IBCAO; Jakobsson et al., 2012) with HALIP localities in black lines (mapped or inferred dyke swarms), and orange and grey polygons (proposed HALIP regions beyond those of dykes) as compiled from various sources (Jowitt et al., 2014; Polteau et al., 2016; Døssing et al., 2017; Minakov et al., 2018); HAMD - High Arctic Magnetic Domain of Oakey and Saltus (2016). The short dashed orange contour is the -2500 m bathymetry line outlining the Alpha-Mendeleev Ridge; the star is the potential arrival site of the HALIP plume; the long dashed white line approximately marks the NW-SE transect traversing from the Amerasia Basin to Sverdrup Basin to the Greenland Craton as used in the numerical models (basin-margin-craton). AHI - Axel Heiberg Island. Note: at the initial HALIP pulse at around 122 Ma (Figure 2), the tectonic configuration was different - the Amerasia Basin was starting to open, the Eurasia Basin did not exist, and Eurekan deformation had not yet occurred.

As with many large-igneous provinces (LIPs) worldwide, a mantle plume is considered to be the primary source of HALIP volcanism. This is supported by several lines of evidence including the widespread distribution of HALIP rocks and the large volume of magmatism (both pointing to a large anomaly of elevated mantle temperatures e.g. (Coffin & Eldholm, 1994; Buchan & Ernst, 2018)), geochemistry containing a primitive mantle and/or recycled oceanic lithosphere component (pointing to a deep mantle source e.g. (Estrada, 2015); though alternative, shallow signals are discussed below), a pattern of radiating and circumferential dykes (pointing to a sub-circular mantle plume head im-

pinging on the lithosphere e.g., Buchan & Ernst, 2018; Minakov et al., 2018), and major regional sedimentary pathway reorganizations in the Barents Sea (pointing to significant relative uplift to the north e.g. (Midtkandal et al., 2020)). The arrival location of the HALIP plume at approximately 130 Ma (Figure 2), is often reconstructed offshore, in the region of the Alpha Ridge (e.g., Buchan & Ernst, 2018) or Lomonosov Ridge (Jackson et al., 2010). Unlike many other LIPs, HALIP does not have a clear hotspot track, though it may be linked to later Iceland plume dynamics and a potential trajectory beneath Greenland (e.g., Lawver & Müller, 1994). It is also worth noting that these observations are complicated by a complex tectonic setting, with the the near-contemporaneous opening (including episodes of rifting, hyperextension and/or seafloor-spreading) of the Amerasia Basin to the north, as well as the later Eurekan deformation event (or orogeny) which affected much of the eastern Canadian Arctic Islands, Northern Greenland, and Svalbard (e.g. (Pease et al., 2014; Shephard et al., 2013)).

Alternatives to a mantle plume origin of HALIP-magmatism have been proposed, at least to account for the later (post ∼120 Ma e.g., Dockman et al., 2018) phases of HALIP (second and third pulse at about 95 Ma and 81 Ma, Figure 2) and therefore its protracted nature as a whole. Edge driven convection (as related to the inherted lithospheric structure of region) is the dominant process invoked. Rifting of the Amerasia Basin (e.g., Tegner et al., 2011) or even Labrador and Baffin Bay rifting (e.g., Thorarinsson et al., 2011) with associated decompression melting are also sometimes invoked as possible mechanisms for some of the HALIP magmatism. For the Canadian Arctic Islands region, Dockman et al. (2018) questioned the need for a plume for the younger phases of HALIP, calling upon multi-phase (decompression) melting and thermal erosion related to edge-driven convection with or without shear, although they do not rule out that a plume may have influenced the asthenospheric flow. However, general modelling studies such as by Manjón-Cabeza Córdoba and Ballmer (2021, 2022) show that edge-driven convection can only rarely produce and sustain magmatism, and generated volumes of magma are small.

Thus whether the HALIP rocks and their origins should be sub-divided temporally, geographically or by mechanism remains an active question discussed within the Arctic geoscience community. Here we return to a plume hypothesis, and propose that its arrival drives HALIP magmatism as a whole. A key question is therefore, can plume-lithosphere interactions explain the long-lived volcanism and pulses observed for HALIP? A regionally-focused study is therefore pertinent; focusing on the HALIP localities in the Canadian Arctic Island therefore offers an opportunity to evaluate the contributions from both shallow and deeper mantle sources, as well as the temporal characteristics of melting. Furthermore, numerical models of mantle convection, which incorporate plume and lithospheric dynamics have never been applied to the High Arctic LIP. In this paper, we suggest that a plume interacting with pre-existing lithosphere-asthenosphere boundary (LAB) topography across the Arctic can produce prolonged and pulsating magmatism across a large area, while other mechanisms may play a secondary role in the emplacement of HALIP.

2 Constraints on the timing and geochemistry of HALIP magmatism

Documented ages of HALIP magmatism spread over a temporal range of ca. 50+ Myrs, from $\sim 131 - 85$ Ma, with a potential peak phase around 122 Ma. If Kap Washington volcanics of northern Greenland ($71 - 61$ Ma Estrada et al., 2010; Tegner et al., 2011; Thorarinsson et al., 2011) are also included, then this time frame increases to over 70 Myrs. The protracted and/or multiple pulses of HALIP pose a particular challenge because most traditionally-defined LIPs are erupted in a relatively short amount of time ($1 - 5$ Myr for > 75 % of the volume). Could a mantle plume potentially cause over 50 Myr of intermittent and spatially variable melting? A particular element to this complexity is in the geochemical signature of HALIP rocks, which show significant variations in composition between different localities, including those within and between the Canadian and

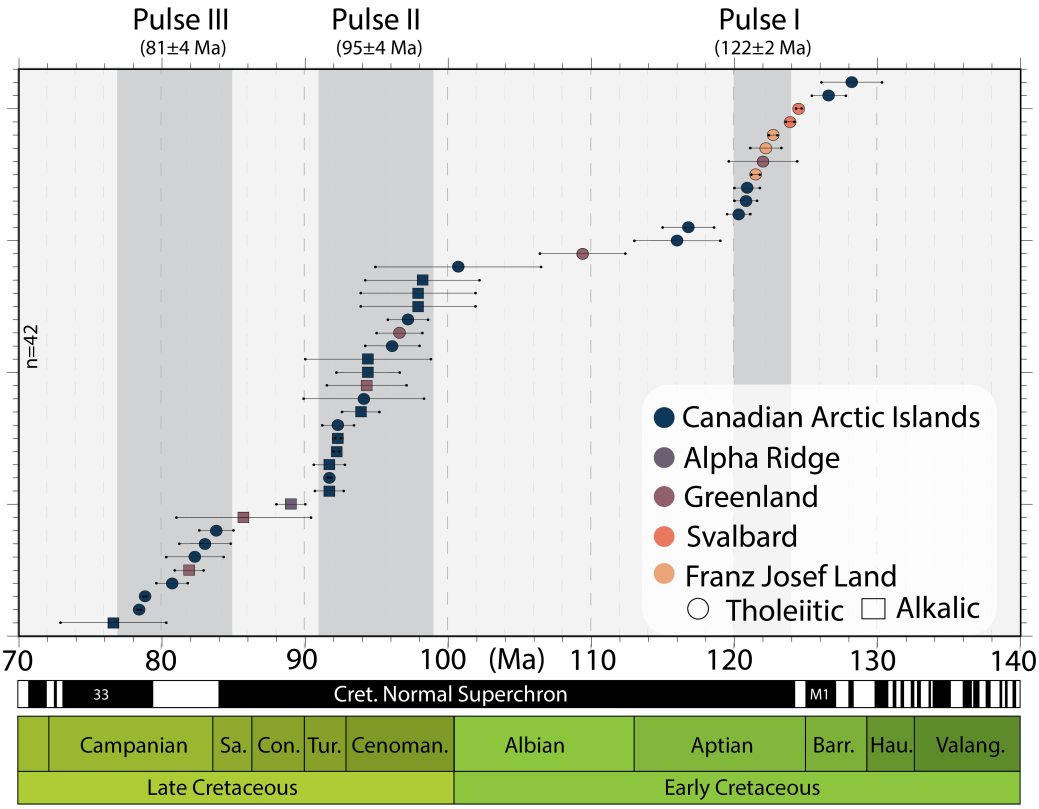

Figure 2: Summary of HALIP dates and the three proposed pulses, coloured by Arctic location and divided into tholeiitic (circle) and alkaline (square) samples with 2 sigma error. Redrawn from the compilation of Dockman et al. (2018), which was in turn based on U-Pb and 40Ar/39Ar studies of Corfu et al. (2013); Estrada (2015); Estrada and Henjes-Kunst (2004); Evenchick et al. (2015); Jokat et al. (2013); Kontak et al. (2001); Villeneuve and Williamson (2006).

Eurasian sectors, and similar sample ages. Broadly speaking, there seems to be consensus that an upwelling mantle plume was involved (albeit the more ambiguous terms "asthenospheric upwellings" or "decompressional melting" are sometimes referred to). However, there is significant geochemical heterogeneity pointing to one, more or all of the following contributions: a heterogeneous mantle plume (e.g. ocean island basalt or recycled oceanic crust signals), crustal contamination, entrainment of sub-continental lithsopheric mantle (SCLM), and/or an enriched sub-lithospheric fossil subduction zone from a nearby subducted slab (metasomatic signal e.g., Shephard et al., 2016; Hadlari et al., 2018).

The arrival of a mantle plume is typically associated with (continental or oceanic) flood basalts and tholeiitic suites, with alkaline magmatism frequently pre-, syn- or post-dating this. Alkaline magmatism in continental settings may form distally to the main zone of extension (or the mantle plume) and can often be used to test whether the same mantle is sampled between tholeiitic and alkaline suites. The later alkaline suites of HALIP appear to be more low-degree mantle melts (Bédard et al., 2021) and/or deeper sourced (Dockman et al., 2018) as compared to their tholeiitic counterparts. The alkaline sites are also regionally confined towards the east (not found in Axel Heiberg Island), with

the extrusive alkaline lavas only found in the northern part of Ellesmere Island (e.g., Trettin, n.d.; Dockman et al., 2018) It is important to further summarize the geochemical heterogeneity here in the context of underlying melt-inducing processes and tectono-magmatic origins, and therefore the definition of HALIP.

The Sverdrup Basin is a ca. 1000 km along strike Carboniferous to Paleogene rift basin at the northern edge of the North American continent, and encompasses Ellesmere, Axel Heiberg and Melville islands, amongst others (collectively the Canadian Arctic Islands). The basin includes changes in crutal (Figure 3a) and lithospheric thickness (Figure 3b) from north to south that reflect its long-lived tectonic history, and likely existed in the past as well. Recent field campaigns also revealed varied geochemical and isotopic signals from HALIP. While dating methods vary, Dockman et al. (2018) summarized three pulses of Canadian HALIP magmatism; $124-120$ Ma, $99-91$ Ma, and $85-77$ Ma. As in other HALIP localities, they are dominated by tholeiitic-type rocks, such as the Isachsen Formation. These are proposed to have an enriched mantle (EM)-like signature and widespread crustal contamination (e.g., Naber et al., 2020; Bédard, Saumur, et al., 2021). However, there are also least two younger groups of alkaline rocks in the Sverdrup Basin region, which are much smaller in volumes. Dockman et al. (2018) describe an overlap period of tholeiitic and alkaline magmatism from ca.100-85 Ma. As recently detailed in Bédard, Saumur, et al. (2021); Bédard et al. (2021), these alkaline suites include the $\sim$96 Ma Fulmar Suite (including Strand Fjord formation), which are suggested to resemble EM-type ocean island basalts with little crustal contamination and a widespread source (apatite-rich) similar to the dominant tholeiites. That said, however, the Fulmar Suite includes Hassel Formation rocks which exhibit a depleted lower crust signal. Two additional, geochemically-similar alkaline suites include the $92-93$ Ma Wootton Intrusive Complex with plutonic rocks and the $83-73$ Ma Audhild Bay Suite (also referred to as the Hansen Point volcanics) with mafic alkaline rocks. These younger localities are thought to resemble HIMU ocean island basalts but with some crustally derived signals, including potentially shallow melting due to flat heavy rare earth profiles. Bédard et al. (2021) concluded that northern Ellesmere Island magmas are derived from variably sampled heterogeneous regions in the sub-continental lithospheric mantle, and do not rule out a mantle plume source.

This geochemical diversity emphasizes the unique characteristics and challenging nature of disentangling shallow-and-deep HALIP processes. Perhaps unsurprisingly, an ocean basin to rifted margin to cratonic margin setting, which has undergone several phases of tectonic events, has a significant amount of structural and compositional variation in its crust and lithosphere (Figure 3). This heterogeneity may in turn have been reactivated or sampled during the more complicated processes of magma migration and fractionation, especially during successive melting episodes.

3 Methods

In order to investigate the dynamics of plume-lithosphere interactions of HALIP, we run 2-D numerical models of mantle convection in Cartesian geometry. We focus on modelling the presence of melt and test the impact of variable lithosphere thickness on melt generation relevant to the emplacement of HALIP. Modelling is done using the open source finite element code ASPECT v2.4.0 (Kronbichler et al., 2012; Dannberg & Heister, 2016; Heister et al., 2017; Bangerth et al., 2022), which includes melting/freezing and melt migration under Darcy's law, and heat advection by melt (Dannberg & Heister, 2016; Dannberg et al., 2019). Since we focus on upper mantle dynamics, the effects of compressibility and depth-dependence of parameters except for viscosity are small (Albers & Christensen, 1996), hence we can use the Boussinesq approximation of incompressibility. We build on earlier 2-D models described in (Heyn & Conrad, 2022) with additional initial conditions and further complexities of melting / freezing and melt migration, as described below.

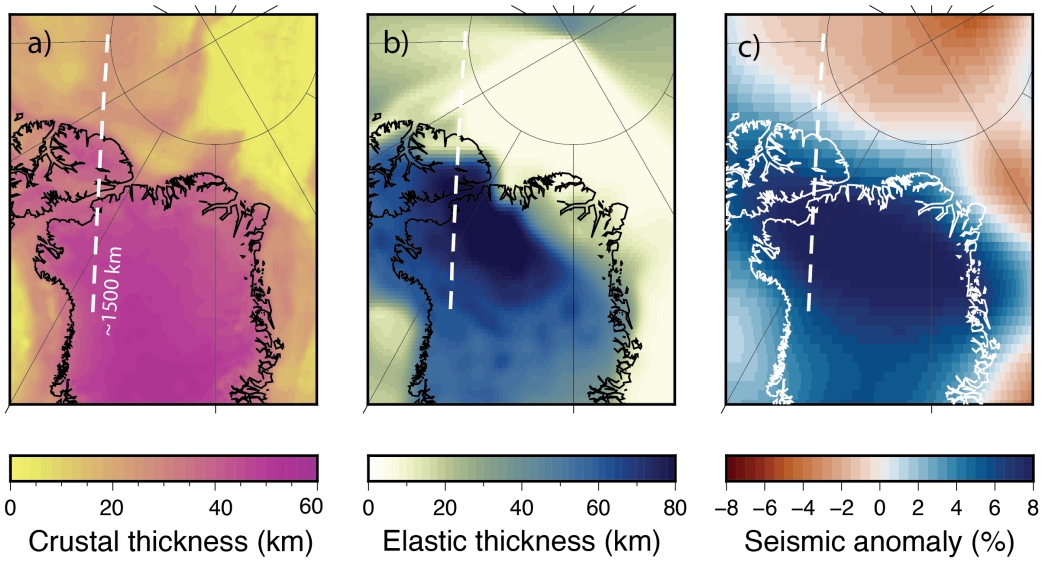

Figure 3: Geophysical datasets for the Canadian Arctic Island and Greenland region overlain with 1500 km transect from Figure 1 (white dashed line). a) Crustal thickness from ArcCRUST (Lebedeva-Ivanova et al., 2019), b) elastic thickness from (Steffen et al., 2018), and c) P-wave seismic velocity anomaly at 150 km depth from SL2013sv (Schaeffer & Lebedev, 2013)

To capture the proposed arrival location of the HALIP plume, we have chosen an approximately NW-SE transect (present-day coordinates) which traverses the (incipient) Amerasia Basin, the Sverdrup Basin of the Canadian Arctic Islands, the cratonic Canadian shield and the northernmost Greenland craton. Two sets of domain sizes are run, and were chosen to minimize boundary effects, while keeping domains small enough to limit computational costs, as well as allow for a systematic study of different boundary conditions and plate configurations. In the horizontal direction, models have extents of either 1500 km or 4000 km, with a vertical dimension of 600 km or 800 km, respectively. The larger domains are necessary for models with a moving plate. We use adaptive mesh refinement to resolve melt migration, with resolution varying between about 25 km in areas of the upper mantle away from the plume, to about 3 km along the surface, the lithosphere-asthenosphere boundary (LAB) and within the mantle plume. Regions with active melting can have higher resolution, depending on melt fractions and melt velocity.

Since the tectonic history of the Arctic and the relative motion of plates and the mantle plume are not well constrained, a useful first approximation for HALIP might be a model with a mantle plume arriving under a stagnant tectonic plate (no-slip conditions). This simulates a scenario in which there is no relative motion between the plume and the plate, but does not necessarily imply that there was no plate motion at all. However, the Arctic was actively undergoing tectonic motions including spreading and extension during HALIP emplacement. Furthermore, it has been suggested that the plume later passed underneath Greenland (e.g., Steinberger et al., 2019; Martos et al., 2018), so it seems likely that there has been a relative motion between the plate and the plume. Therefore, we investigate models with 2 different scenarios:

1. cases with stagnant plate: model domain with dimensions of 1500x600 km, up to two steps in lithosphere thickness, zero-slip boundary condition at the surface and free-slip for all other boundaries

2. cases with imposed plate velocity: model domain with dimensions of 4000x800 km, up to two steps in lithosphere thickness moving over the plume, an imposed plate velocity of 2 cm/yr at the top, imposed plate velocities at the side walls to balance inflow and outflow, and free-slip at the bottom

For both scenarios, the temperature is fixed along the top and bottom boundary to 273 K and 1623 K, respectively, and the initial temperature is described by a linear gradient within the lithosphere of thickness d (defined by the 1400 K isotherm), and a linear gradient from the base of the lithosphere to the bottom of the domain. Present-day estimates of lithospheric thickness (Figure 3b) and upper mantle structure (Figure 3c), constrained using seismic and gravity data, vary significantly across our transect . Due to the long-lived and multiple-phases of regional tectonic deformation, it is likely that similar lithospheric heterogeneity existed also in the past. To account for this, the lithosphere thickness d within the models at the starting condition varies between at least 50 km in the extended basin north of Greenland and up to 200 km for the Greenland craton. The transition between the basin and the craton is simulated by either a gradual increase or up to two 'steps' in the depth of the LAB. Details of the model setup are shown in the next section when the respective model results are discussed.

In order to simulate a (thermal) mantle plume, a plume seed is added to the temperature field as a Gaussian-shaped anomaly of excess temperature 250 K, both as temperature boundary condition kept during the run, and as part of the initial condition within the lowest 50 km of the domain. Models are run going forward in time for 150 Myr, which should be sufficient to capture the HALIP melting dynamics. For models without imposed plate velocity, the plume seed is removed after 75 Myr in order to limit potential melting times to a duration relatable to HALIP (see e.g. Figure 2).

Viscosity is known to be a key parameter for mantle convection, and it has been shown to play a major role in plume-lithosphere interaction and the amount of lithosphere thinning associated with the plume (Heyn & Conrad, 2022). Since the presence of melt will reduce the overall viscosity of the respective region, viscosity is implemented into the model as a modified diffusion-dislocation creep that includes the effect of melt following Dannberg and Heister (2016), and a step below the asthenosphere:

$$\eta_{\text{eff}} = \frac{\eta_j}{\eta_{\text{ref}}} \left(\frac{1}{\eta_{\text{eff}}^{\text{diff}}} + \frac{1}{\eta_{\text{eff}}^{\text{disl}}} \right)^{-1} \cdot \exp\left(\alpha_\phi \phi\right) \cdot \exp\left(\alpha_\psi \psi\right) \tag{1}$$

with

$$\eta_{\text{eff}}^{i} = \frac{1}{2} A^{-\frac{1}{n_i}} d^{\frac{m_i}{n_i}} \dot{\epsilon}_i^{\frac{1-n_i}{n_i}} \exp\left(\frac{E_i + PV_i}{n_i RT} \right). \tag{2}$$

Parameters in equation (2) are the prefactor A, the stress exponent n, the grain size d, the grain size exponent m, the strain rate $\dot{\epsilon}$, the activation energy E, the activation volume V, and the gas constant R. P and T describe pressure and temperature, and the index i refers to either diffusion or dislocation creep. In equation (1), η_j and η_{ref} give the viscosity prefactor for layer j and the reference viscosity used to implement the viscosity jump underneath the asthenosphere. The exponential terms describe the weakening effect of melt with melt fraction ϕ (i.e. the porosity field) and exponential prefactor α_ϕ, and the strengthening effect of melt depletion via the fraction of melt residue ψ (i.e. the positive peridotite field) and the corresponding exponential prefactor α_ψ, which is in this case set to 0 (no depletion strengthening). In analogy to Heyn and Conrad (2022), we simplify this viscosity law to a temperature and composition dependent rheology with $m_i = 0$, $n_i = 1$ and $V_i = 0$. All values for the parameters are listed in Table 1.

Melting and freezing are calculated relative to the dry solidus following Dannberg and Heister (2016), defined by the surface solidus and the pressure gradient given in Table 1, as

$$T_{\text{sol}} = T_{\text{sol},0} + \Delta T_p p + \Delta T_\psi \psi \tag{3}$$

Table 1: Characteristic parameters used in the numerical simulations that are referred to in the text. The solidus pressure gradient is given for the different models in the order they are mentioned in the text, i.e. "2 steps stagnant plate", "2 steps moving plate", "1 ramp moving plate", "a step moving plate", and "2 steps symmetric moving plate". To see a full list of parameters, including those remaining at the default value specified in the material model, readers are advised to look at the provided parameters files and material model plugin for ASPECT.

Parameter	Symbol	Value [Unit]
Gravitational acceleration	g	9.81 [m/s^2]
Reference density	ρ	3300 [kg/m^3]
Surface velocity (moving plate cases)	v	2 [cm/yr]
Reference viscosity	η_{ref}	$1 \cdot 10^{22}$ [Pa·s]
Viscosity prefactor for upper/ lower layer	η_j	$5 \cdot 10^{22}$/ $1 \cdot 10^{24}$ [Pa·s]
Prefactor melt weakening	α_ϕ	27
Prefactor depletion strengthening	α_ψ	0
Viscosity prefactor	A	$8 \cdot 10^{-12}$ [1/Pa·s]
Stress exponent	n_i	1
Grain size exponent	m_i	0
Activation energy	E_i	250 [kJ/mol]
Activation volume	V_i	0 [m^3/mol]
Surface solidus temperature	$T_{\text{sol},0}$	1350 [K]
Solidus pressure gradient	ΔT_p	7.8/ 6.8/ 9.0/ 7.8/ 7.8 $\cdot 10^{-8}$ [K/Pa]
Solidus depletion change	ΔT_ψ	200 [K]

via the surface solidus $T_{\text{sol},0}$, the pressure gradient ΔT_p and the depletion change ΔT_ψ, with the the pressure p and the depletion (positive peridotite field) ψ. Hence, melt depletion increases melting temperatures. Once melting has occurred, active melt and melt residues are tracked via compositional fields termed 'porosity' and 'peridotite'. While porosity tracks the active melt fraction (and is therefore always positive), peridotite refers to the fraction of mantle material that has been affected by melt. Therefore, it can have either negative values (for enriched material representing recrystallised melts) or positive values (for melt-depleted material). The migration of melt, which includes heat advection, is modelled via two-phase flow according to Darcy's law, assuming that melt moves through pore spaces of the mantle. As a consequence, no magma chamber can form, and the effect of Earth's rotation can be neglected. Instantaneous melt volumes at any given time can be obtained by integrating the porosity field over the domain, and time-integration results in cumulative melt volumes. However, since melting and freezing happen on much shorter time scales than mantle convection, both melt volume calculations based on the porosity field may not be able to capture all melt produced during the model runs, and therefore only provide first-order estimates of melt volumes. Furthermore, modeled melt volumes strongly depend on the surface solidus and the pressure gradient, which are not well constrained and vary between the models to avoid extreme melt fractions.

Having described the relevant governing equations and technical terms above, it is important to establish and clarify some definitions. In the following text, melt refers to the active melt fraction at any given time step as obtained from the porosity field. Melt that cools down and freezes is not included. Based on the average melt fraction per model cell and its area, we can calculate the total 'melt area', which is technically not a volume since models are 2-D. To convert this into volume estimates, we assume that the model cells are 1 km deep with no variation of melt fraction along this direction, result-

ing in volumes of "km^3 per km assumed model extent". Note, however, that this approach cannot represent real 3-D melt volumes, but is likely to underestimate actual melt volumes because melting areas are typically larger than 1 km in each direction. Therefore, we use calculated cumulative (time-integrated) and peak instantaneous melt volumes only as comparison between different models (as far as the parameters allow), but do not compare them with estimates of erupted or intruded melt for HALIP. In addition, these models do not 'erupt' the melt onto the surface of the model (e.g. via extrusive volcanism) nor assume any removal of melt as done in other studies that calculate "simplified" melt fractions as postprocessing step (e.g., Ballmer et al., 2011; Bredow et al., 2017; Steinberger et al., 2019) - the difference between these types of model and models with melt migration are discussed in sections 5 and 6. The reason that mantle convection models do not include actual eruptive volcanism, and few include melt migration at all, is that the computational effort needed to bridge the time and length scales of larger scale mantle convection and eruptive modelling is expensive. This study serves therefore as a first-order estimate on the spatial and temporal dynamics of plume-lithosphere interactions in the presence of melt migration. For nwo, we simply assume that part of the melt will reach the surface and erupt to form HALIP's extrusive magmatism.

4 Results of plume-lithosphere interaction with melt migration

The basic plume-lithosphere interaction for melt-free models including their parameter dependence has been discussed in (Heyn & Conrad, 2022). Here, we added more complexity by including melt migration and non-uniform lithosphere thickness to see whether the interaction of lithospheric steps can explain all or part of the multi-pulse melting behaviour and complexity of HALIP. For simplicity, we will first analyse a model with a stagnant plate, before considering moving plate scenarios.

4.1 Stagnant plate with 2 lithospheric steps

In order to simulate the transition between a continental edge to a more cratonal interior, i.e. from the Sverdrup Basin to the cratonic parts of Greenland, we implemented two lithospheric steps 500 km apart from each other, increasing the lithosphere thickness from 100 km in the northwest (Sverdrup Basin) to 200 km underneath the Greenland craton in the southeast (see Figure 4a). For the initial condition, the plume is placed underneath the first step (towards the left of the domain, representing the northwestern part of the transect), such that it interacts with the lithosphere close to the modelled margin of the continent. The existence of melt at a given time step is indicated by the melt fraction in Figure 4c, which is plotted on top of the temperature field. The first melt appears after about 12 Myr of model time (Figure 4b), when the plume head ascends and reaches a depth of about 200 km. However, initial melt fractions are small and focused in the top area of the plume head (indicated by the black pixels Figure 4c). Within the next $1-2$ Myr, the plume head reaches the LAB, and tilts to the left/northwest, towards the thinner lithosphere of the Sverdrup Basin, resulting in strongly asymmetric spreading of the plume material. This asymmetry becomes more pronounced over time, with significantly less plume material spreading below the margin (second step, e.g. visible after 21 Myr).

In this model, melting only occurs beneath the left/northwestern part of the domain (4c), and its distribution varies significantly with time and space (4b,c). Within just 1 Myr (between 12 and 13 Myr), the melt initially generated in the central portion of the plume head (12 Myr) has risen advectively and reached the LAB. This interaction generates significantly more melt by 13 Myr due the the heat advected with the rising melt and a lower solidus temperature of the ambient material. Additionally, at 13 Myr, a second melting area to the left/northwest has formed in another branch of the plume head around $100-200$ km away. This is separated from the older central melt region

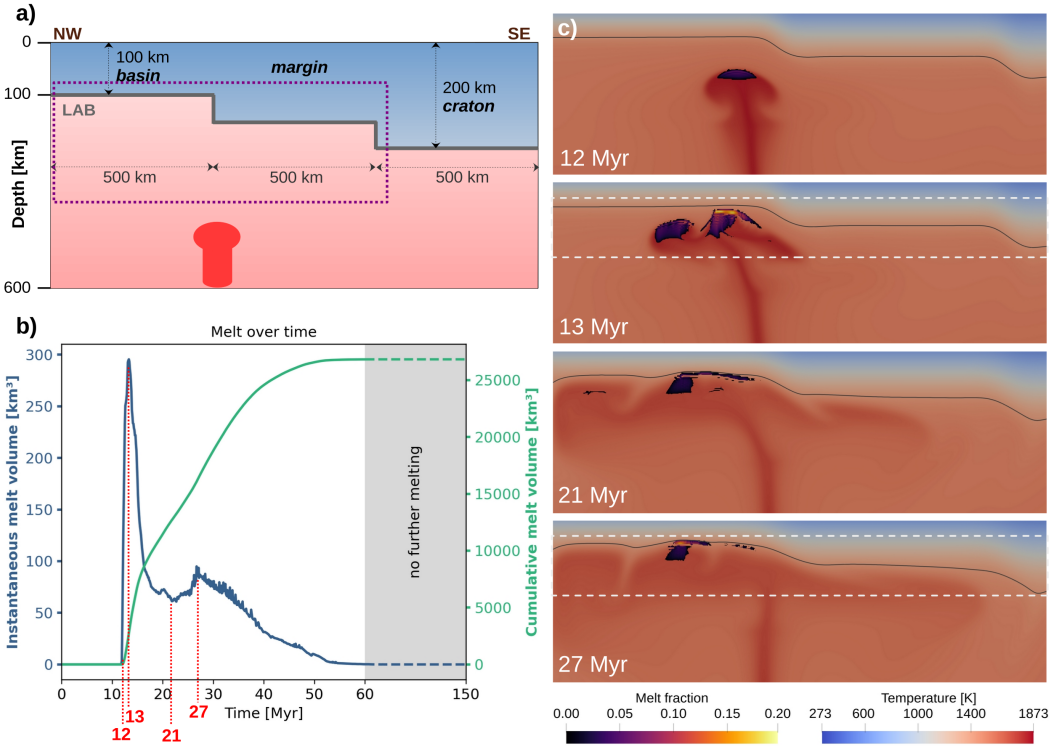

Figure 4: Results for a 2-D model with 2 lithospheric steps and a stagnant plate, with (a) the model setup including domain dimensions, (b) the instantaneous and cumulative melt volumes over time, and (c) selected snapshots of the temperature field (blue-red colours) overlain with active melt fraction (black-magenta-yellow colours). The lithosphere-asthenosphere boundary (LAB, corresponding to the 1400K isotherm) is indicated in (a) and (c) by the dark line. The calculated instantaneous melt volumes in (b) correspond to the integrated melt fractions shown in (c) at the indicated times. Note, however, that 2-D models do not give actual melt volumes, but rather 2-D "melt areas" in km^2, which are then for simplicity converted to melt volumes assuming an extent of 1 km in the third dimension (see section 3 for more information; a more appropriate term could therefore be "melt volumes per km"). The purple dotted rectangle in (a) marks the zoom-in of the domain shown in (c), and the time-evolution of melt volumes in (b) is compressed after 60 Myr since no more melt is generated in the model. White dashed boxes mark the zoom in for Figure 6.

by a downwelling due to local small-scale convection. The downwelling migrates to the left with time, and is also visible at 21 and 27 Myr. By 21 Myr, the total amount of melt has decreased significantly (indicated by lack of purple/yellow colours in Figure 4c and the melt volume in Figure 4b), with the second melting region being almost melt-free, and the initial melting area being spread out and directly interacting with the LAB. Due to the erosion of the lithosphere by melt-induced small-scale convection, the initial melting region experiences rejuvenated strength of melting by about 27 Myr (Figure 2b and 4c, lowermost panel). After this episode of rejuvenated melting, the amount of melt in the model subsides, and the model reaches a melt-free state from about 50 Myr. Even though the mantle plume is still active (switched off at 75 Myr), it does not initiate further melting, neither above the plume nor in any of the previous melting regions. For this model, the duration of melting is ca. 38 Myr (from 12 – 50 Myr).

4.2 Moving plate with 2 lithospheric steps

As a next step, we introduce a plate moving with a constant velocity of 2 cm/yr towards the left/northwest, such that the cratonic part of the model eventually moves towards and over the plume. The initial setup is similar to the case shown in Figure 4a, but the model domain is extended towards the north, with the steps starting 300 km and 800 km right/southeast of the plume position (see Figure 5a). The distance to the first step is chosen so that the plume head hits the transition between the basin and the continental margin, similar to the stagnant plate case. The first melting occurs at around 14 Myr (Figure 5b), and increases significantly until the plume head hits the LAB at 15 Myr, just in front of the first step where the basin transitions to the margin (Figure 5c). The instantaneous melt volume at the peak of this initial pulse is around 520 km^3 compared to 300 km^3 in the stagnant scenario, but the cumulative melt volume is much bigger for the stagnant plate case (about 26,800 km^3 for stagnant plate vs. 15,900 km^3 for moving plate). The plume and region of melt at this time, and after, is tilted and deflected towards the left/northwest, towards the thinner lithosphere of the basin. As in the stagnant plate model, the resulting time-dependent melt distribution is spatially inhomogeneous. From ca. $15-21$ Myr there is a large amount of melting occurring close to the continental margin (first step), and a second melting region is developing about 500 km away from the step to the left/northwest, underneath the basin. With increasing time, the steps move towards the northwest relative to the plume, and at 21 Myr, the continental margin begins to pass over the underlying plume position.

At around 35 Myr, the plume material, as indicated by both the thermal and melt fraction fields, covers an area extending more than 1000 km away from the active plume, which is now located under the second step (craton). At this time, there is no more melting occurring in the model. However, over time, the topography of the LAB has facilitated the channelling of the shallowest plume material to the left/northwest, towards the thinner lithosphere of the basin. A result of this is that around 45 Myr, plume material arriving at the southeastern edge of the basin in front of the first step is hot enough to melt, causing "rejuvenated" melting underneath the same region of the basin that has previously been affected by melting when the plume head arrived at 15 Myr. This melting occurs in two small pockets, separated by a small downwelling, and is related to local small-scale dynamics of plume material interacting with locally thinned lithosphere. Note, however, that the melt fractions and the amount of melt are much smaller than for the first batch of melting (about 0.013 maximum melt fraction and 300 km^3 cumulative volume compared to 0.23 maximum melt fraction and 15,600 km^3 cumulative melt volume, respectively). It is also worth noting that this "rejuvenated" melting in this model (c.f. the second pulse at 27 Myr in the stagnant case) lasts for at most 10 Myr and happens approximately 30 Myr after the initial melting (see Figure 5b). As will be discussed later in more detail, both the length, timing and position of rejuvenated volcanism correspond to the constraints from HALIP data for the first and second pulse of magmatism obtained from Dockman et al. (2018, see also Figure 2), while relative volumes for HALIP are extremely difficult to quantify and may not be represented correctly in the models. Finally, it is noteworthy that the melting at this time occurs more than 500 km away from the active plume stem, indicating that the presence of melt cannot necessarily be used as a constraint for the central plume position at the given time. The duration of melting in this scenario is ca. 21 Myr (from $14-35$ Myr) or ca. 33 Myr ($14-47$ Myr) if considering the later, distal episode.

4.3 Lithosphere thinning and its relation to melting regions

As described in Heyn and Conrad (2022) for melt-free models (i.e. neither simplified melt fractions nor migration included), the lithosphere above a mantle plume starts to thin as soon as the plume head reaches the lithosphere-asthenosphere boundary due to thermo-mechanical erosion from the plume. With continued plume-lithosphere inter-

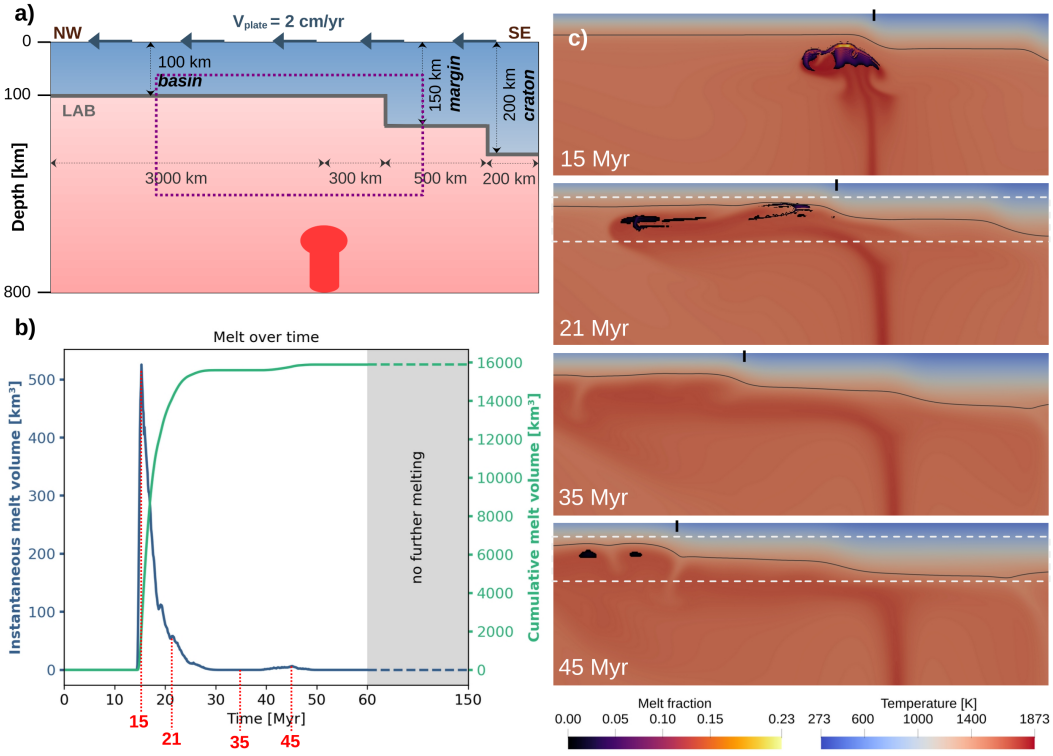

Figure 5: Model setup for a case with 2 lithospheric steps in which the craton moves over the plume with an imposed plate velocity of 2 cm/yr indicated by arrows (a), instantaneous and cumulative melt volumes versus time (b), and temperature field snapshots with porosity for given times (c). As for Figure 4, the rectangle in (a) marks the area of the temperature snap shots shown in (c), and times from the snap shots in (c) are marked for the instantaneous melt volume in (b). The edge of the basin is marked by the small black vertical line, and the dashed white boxes mark the zoom in used for Figure 6. In contrast to the stagnant plate case, this model reaches a melt-free stage at about 35 Myr, before "rejuvenated" melting occurs at around 42 Myr underneath the right/southeastern corner of the basin.

action, the local thinning becomes more pronounced, reaching a maximum value shortly after the plume is removed (for stagnant plate cases) or the respective plume-affected area of the lithosphere has moved significantly (about 200−300 km) relative to the plume (for moving plate cases). In contrast to the melt-free models of Heyn and Conrad (2022), we find that melt rising from the melting zones in the plume head can further reduce lithosphere thickness locally. Figure 6 plots the amount of lithospheric thinning occurring across the horizontal direction at two selected time steps for the two models with two lithospheric steps as discussed above (c.f. Figures 4a and 5a). These particular time steps were chosen because they correspond to changes in the melt fraction (e.g. panel b Figure 4 and 5). As seen in Figure 6a for the stagnant plate model (corresponding to Figure 4), thinning starts at 13 Myr above the melting region (rightmost corner of the basin, next to the first step), but the effects are small since the melt has just reached the LAB. The presence of melt, and its ability to rise faster than the rest of the plume, reduces local viscosity, increases local dynamics and therefore causes local erosion while a plume with simplified melt fractions at the same point is starting to spread out at about 50 km below the LAB (compare Figure 9a). At 27 Myr, the lithosphere is thinnest above the leftmost part of the prolonged primary melting region, where melting is still active (c.f. Fig-

ure 4c), while the lithosphere thickness is less affected above the second melting region further left/northwest and the area closer to the step where only a small amount of melt remains.

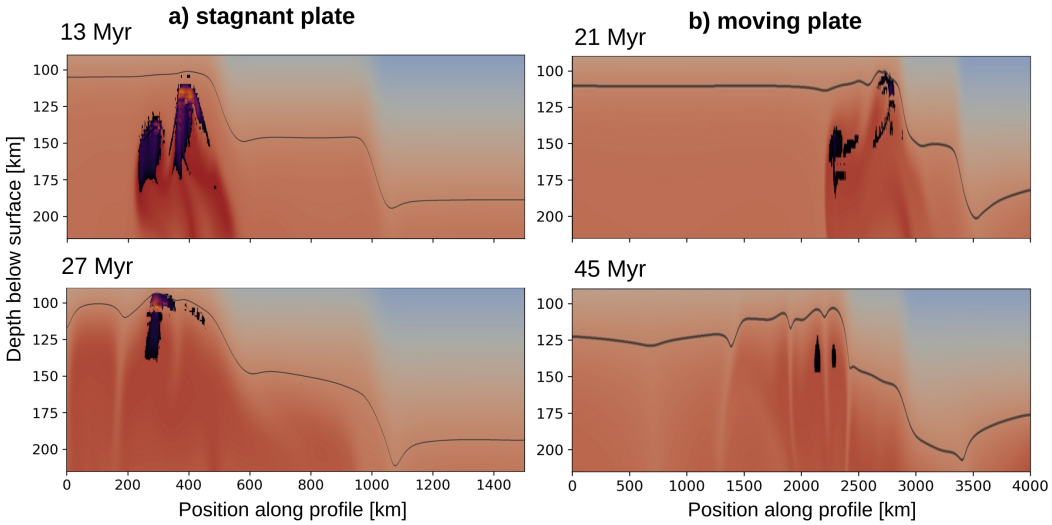

Figure 6: Depth of the LAB (defined as the 1400 K isotherm) at given times for the models with two lithospheric steps discussed above, with the (vertically stretched) temperature fields and melt fractions from Figures 4c and 5c added. While the arrival of melt at the LAB at 13 Myr in (a) only causes a small reduction in thickness, this effect is significantly more pronounced at later times. Small-scale undulations are related to the presence of melt, and are therefore absent underneath the thicker parts of the lithosphere where no melting occurs.

A similar observation can be made in Figure 6b for the moving plate case (corresponding to Figure 5). At 21 Myr, melting is still active the in the primary melting zone close to the step, where the lithosphere is significantly thinner than it is further away from the plume. The melting region further to the left/northwest (which did not reach the LAB in Figure 5c at 21 Myr) seems to have little effect on lithosphere thickness at this particular time step. After melting ceases, the lithosphere starts to heal and increases in thickness, as expected. Yet, some of the melt-induced undulations of the LAB remain, and local dynamics can reactivate these areas at 45 Myr. Even though melting itself happens at about 125-150 km depth, the presence of a thinned lithosphere enables local convection that brings plume material up into the melting zone. Note, however, that the local thinning of the lithosphere by melt is limited both in space and time, and reflects the amount of melt that was locally present. As a consequence, the lithosphere beneath the thicker continental margin or the craton to right of the plume is significantly less affected than the lithosphere beneath the basin, and LAB undulations exhibit much longer wavelengths and lifetimes. Since surface heat flux is a time-delayed and long-wavelength filtered image of the lithosphere thinning (Heyn & Conrad, 2022), it does not reflect the deeper, local, time-dependent melt distributions as predicted in these models. However, if melt were to migrate significantly closer to the surface in these models, then it would exert a larger (but still local) effect on surface heat flux.

4.4 Influence of lithospheric structural variations

In order to investigate the robustness of the rejuvenated volcanism for models with a moving plate, we tested three alternative initial LAB topographies; a gradual ramp,

a single step, and an indentation set-up. For the first alternative model, we followed the conceptual model of Dockman et al. (2018), and included a gradual increase of lithosphere thickness from 50 km underneath the Sverdrup basin to 100 km underneath the Greenland craton (see Figure 7a), starting initially 300 km right/southeast of the plume. Due to the reduced lithosphere thickness, we increased the pressure gradient for the solidus to reduce overall melt volumes (see Table 1), while all other parameters are kept constant. As for the case of 2 discrete lithospheric steps (Figures 4 and 5), the initial melting zone in the plume head quickly separates into separate regions (here three), separated by local downwellings (15 Myr, Figure 7c). The peak of melt is the highest for any model, reaching about 700 km^3 at ca. 15 Myr, and the cumulative melt volume of about 28 600 km^3 is also the largest of all models. In contrast to the previous case, the plume head is initially less tilted, and one branch of the plume head with melting forms underneath the lithospheric ramp, resulting in a total of three distinct melting zones. Hence, the larger peak of instantaneous melt volume (also reflected in the largest melt fraction of 0.31) and larger cumulative melt volume may partly be related to reduced overall lithosphere thickness, despite the increased pressure gradient of the solidus, and partly to the flatter LAB topography that allows for a third melting zone (instead of two as in the previous cases). At 21 Myr, the two side branches of melting are stretched significantly and have a larger distance from the central melting zone, while showing only marginal amounts of melt (as indicated by only black pixels). The central melting zone at the base of the ramp (right/southeastern edge of the basin) is no longer above the plume, but still maintains a melt fraction of about 0.15, and instantaneous melt volumes reach a small secondary peak (see Figure 7b). However, with the plate moving further to the left/northwest, melting stops completely and the model becomes melt-free (30 Myr), before the central melting region becomes re-activated around 42 Myr. As before, this rejuvenated melting happens about 25 Myr after the initial melting, with much smaller melt volumes ($\sim$ 250 km^3 cumulative melt volume) and fractions ($\sim$ 0.014) forming over a duration of a few Myr (Figure 7b) and about 600 km away from the plume stem. Hence, multiple melting events can be produced with different initial LAB topographies, as long as the LAB channels plume material towards a thinned area, for example a region that has been influenced by melt before.

Results from two additional model setup scenarios (a single step or 2 steps symmetric around a thinned area, Figure 8) show peak instantaneous melt volumes that are smaller than for the cases discussed above. In these cases, there is not a clear sign of rejuvenated volcanism. Note, however, that for both of these cases the plume stays longer beneath the basin and the pressure gradient of the solidus temperature is increased compared to the case with 2 consecutive steps (see Table 1; the value used is the same as for the stagnant plate case) in order for these models to run without generating $> 50\,\%$ melt fraction, which would make the model numerically unstable. For the single step case (Figure 8b; red line), the lithospheric step to the craton is 500 km away from the arriving plume head, and the extended basin allows the plume material to spread more evenly and easily towards both sides, resulting in an instantaneous melt volume above the plume of about 310 km^3 at 16 Myr. Due to the smaller initial melt volume, the lithosphere is less thinned, and it becomes more difficult to re-activate any melting zone once the plume interacts with the step (craton). In addition, the lithosphere has more time to heal before the plume material is channeled to the left/northwest by the craton. For the model with a gap (two symmetric steps), it may be expected that plume material rising into the gap of continental lithosphere will be trapped there. In this case, prolonged melting periods may be expected, and perhaps also rejuvenated magmatism once the plume moves underneath the continental lithosphere on the other side of the gap. However, our model (Figure 8b; black line) does not show this, potentially because the initial melt volume in the plume head is too small ($\sim$ 240 km^3 at 19 Myr) to cause enough lithosphere thinning for rejuvenated melting.

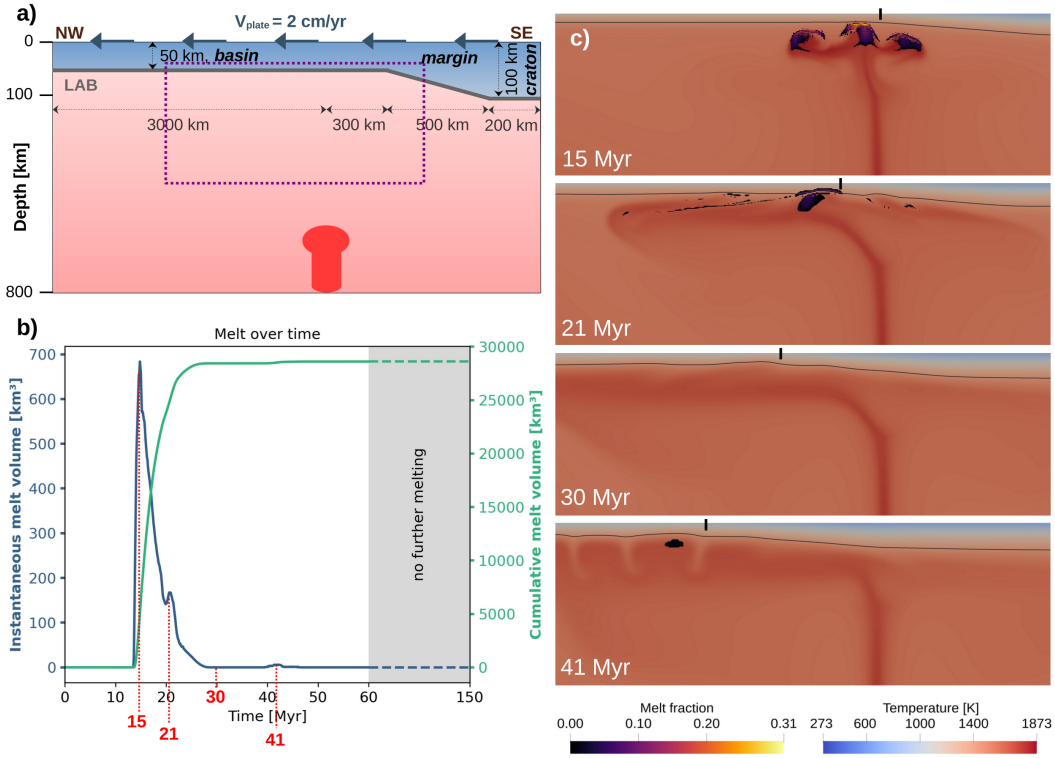

Figure 7: Analogous to Figure 5, but for a model with a gradual transition between the basin and the craton instead of two steps, with the edge of the margin marked by a black vertical line. As before, the imposed velocity is 2 cm/yr, as indicated by the arrows in the model setup (a), and the time evolution of melt volumes is focused on the first 60 Myr (b). As shown in the snap shots of the temperature field (c), the initial melting zone is split into 3 separate branches at 15 Myr, but only the central branch can sustain substantial melting at 21 Myr. At 30 Myr, the model is melt-free, but experiences rejuvenated melting around 41 Myr underneath the right/southeastern part of the basin.

Finally, we compare the results of our cases with variable LAB depth to a case with a moving plate and a constant lithospheric thickness of 100 km, i.e. a model without any cratonic or continental parts interacting with the plume ("uniform LAB" in figure 8a). The pressure gradient of the solidus for this case is set to $7.6{\cdot}10^{-8}$ K/Pa, and instantaneous melt volumes for this model are shown in Figure 8a as the dashed blue line. No second pulse of melting occurs, despite the fact that the instantaneous melt volume associated with the arrival of the plume head ($\sim$950 km^3) is even larger than for the two lithospheric steps or the gradient case, and an overall duration of magmatism of 20 Myr. Since there is no thicker part of the lithosphere moving over the plume, less plume material is directed to a previously thinned area of lithosphere, and melting zones will not be reactivated. Hence, both LAB topography and sufficient initial melting seem to be necessary to generate rejuvenated magmatism.

5 Comparison of melt migration versus "simplified" melt fractions

As far as we are aware, and given our model setup, this work is the first time that rejuvenated melting, unrelated to plume flux changes, has been observed in numerical models. Previous work looking at plume-lithosphere interactions and the emplacement of large igneous provinces (e.g., Steinberger et al., 2019; Duvernay et al., 2022) used "sim-

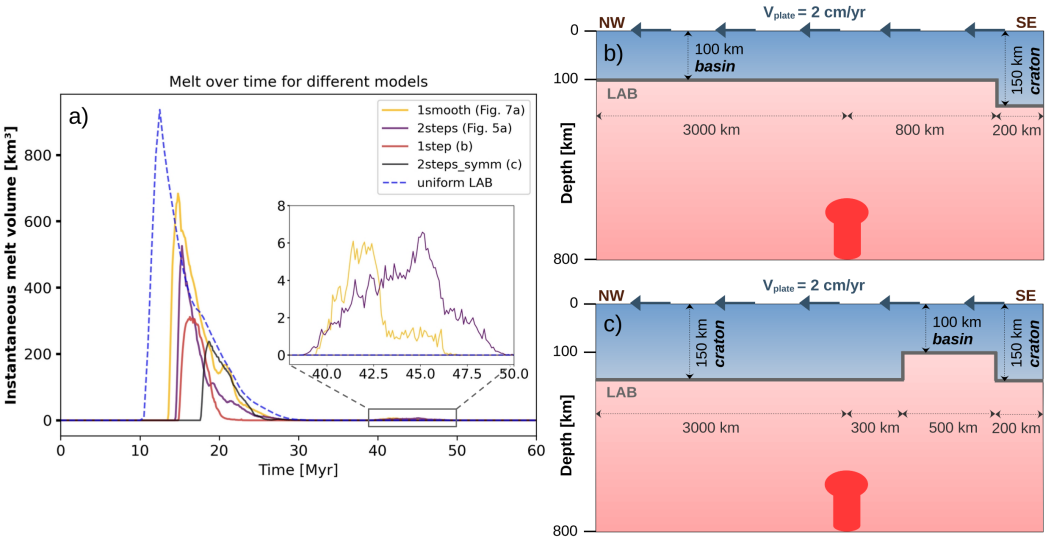

Figure 8: Comparison of instantaneous melt fractions for different initial LAB topographies with a zoom-in to the rejuvenated magmatism (a), and the model setups for a case with one step (b), and 2 symmetric steps (c). Note that the rejuvenated magmatism is only visible for the two lithospheric steps (purple line) shown in Figure 5 and the gradual increase in lithosphere thickness (yellow line) from Figure 7. However, peak instantaneous melt volumes are smaller for the model setups with one step (red line) and two symmetric steps (black line), potentially reducing the chance to observe rejuvenated melting. On the other hand, a model with constant lithospheric thickness (dashed blue line) has the largest maximum instantaneous melt volume of all models shown here, but does not show rejuvenated magmatism. Hence, a large instantaneous melt volume alone seems to be insufficient to generate rejuvenated magmatism if LAB topography is absent.

plified" melt fractions instead of melt migration. Simplified melt fractions are calculated as a post-processing step based on the temperature field, and it is typically assumed that all melt generated at a given time is immediately extracted from the system via volcanic eruptions. In contrast, melt migration involves solving for two-phase flow and the actual migration of material (melt/ residue) and heat - the advantage of this being a much more realistic feedback between melt and local dynamics. On the other hand, the simplified melt fraction approach automatically generates estimations of erupted melt volumes, while the melt migration method does not dynamically erupt any melt and would therefore require the setting of an appropriate threshold to estimate erupted melt volumes. Using melt fractions, the study of Steinberger et al. (2019) investigated how the North Atlantic Igneous Province (NAIP) may have been emplaced by the Iceland Plume interacting with the Greenland craton, and was able to reproduce the reported time frames and melt distributions around Greenland. In contrast, Duvernay et al. (2022) took a more general approach and tested how different settings of lithosphere thickness affect the generation and patterns of simplified melt fractions. Their results show that melt distribution can vary significantly depending on where the plume impinges on the lithosphere, resulting in a very inhomogeneous distribution of the inferred magmatism over time and space. However, neither of their models reproduced rejuvenated volcanism, as has been suggested for HALIP. Based on our models, we suggest that the missing component is the local small-scale dynamics of the melt, which can only be captured by modelling full melt migration. The dynamic feedback between mantle convection and melt is necessary to thin the lithosphere locally enough to facilitate rejuvenated melting, which would otherwise require significant changes in plume strength or lithospheric rifting.

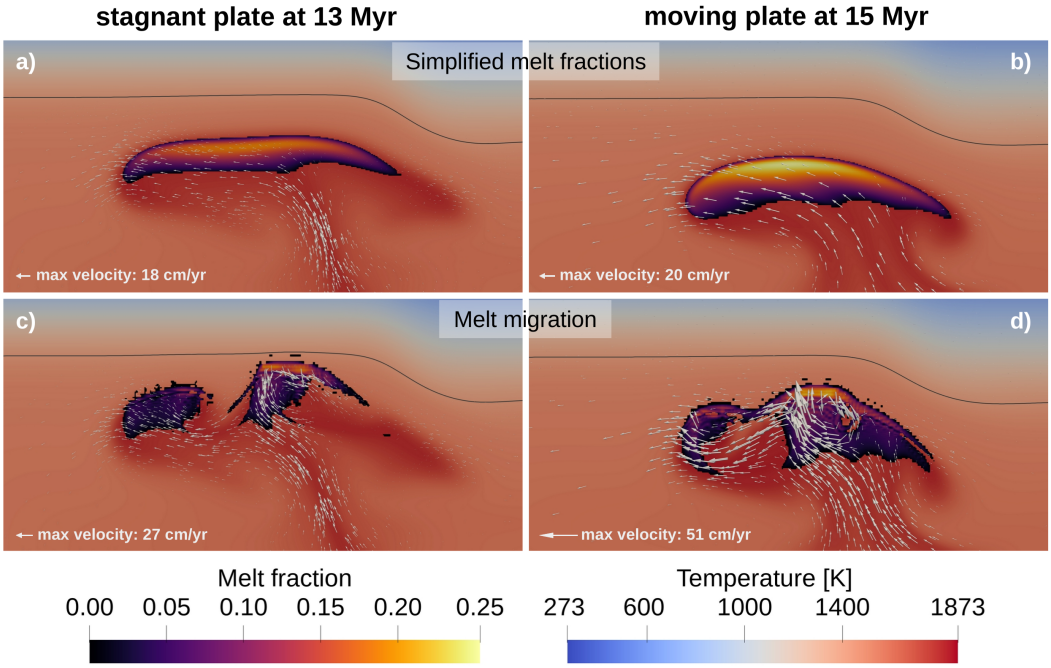

Figure 9: Comparison of 2-D models that implement simplified melt fraction (top row, (a) and (b)) with those that include 2-phase flow melt migration (bottom row, (c) and (d)). Models feature 2 lithospheric steps and either a stagnant plate (left panels (a) and (c), see Figure 4) or a moving plate (right panels (b) and (d), compare Figure 5), and melt is shown on top of the temperature field. Velocities are shown as white arrows, with the scale giving the maximum velocity in each case. While maximum melt fractions are similar in all cases, the melting zones for simplified melt fractions are much broader and more homogeneous than for the cases with melt migration. Note also that plume-related melt in the melt migration cases (bottom row) can rise to shallower depths (compared to the top row, where melting is confined within the plume head), effectively transporting heat to shallower depths.

As mentioned, the calculation of simplified melt fractions happens as a post-processing step, hence the presence of melt does not influence the dynamics. Figure 9 compares models with simplified melt fractions (top panels) to models that include melt migration for two setups: one with a stagnant plate (Figure 9a,c) and one with a moving plate (Figure 9b,d), both with two lithospheric steps. For both the stationary and moving models that only calculate simplified melt fractions (Figure 9a,b), the result is a more homogeneous spread of melting across the plume head. The uppermost edge of the plume head, as indicated by the pattern of the melt fraction field, is more or less parallel to the LAB. Furthermore, the melting zone occupies most of the upper third of the plume head, with the largest melt fractions (yellows) in the upper part of the melting zone. The corresponding mantle flow field shows rising material in the plume stem, which spreads parallel to the lithosphere underneath the basin region, with only a small portion of the plume moving underneath the first lithospheric step to the right/southeast (continental margin). In contrast, melt migration models (lower panels) show two separated or loosely connected melting zones (as described in the above section). Melt generation and distribution are very inhomogeneous, with large melt fractions being much more localized than for the models that exclude melt migration. These local dynamics are driven by density and viscosity variations introduced by melt as it evolves through time. This is also reflected in the velocity field; there is increased flow speed and local upwelling in

regions where larger amounts of melt are being generated. For example, for the moving plate scenario, the maximum velocity is 20 cm/yr for the simplified melt fraction case and 51 cm/yr when including melt migration. In turn, these localized upwellings cause adjacent downwellings, splitting the melting zones and resulting in a small convection cell next the lithospheric step. Maximum melt fractions (i.e. reaching up to 0.25) at this particular time step are comparable between models with and without melt migration, but total volumes of melt differ significantly due to the smaller melting zones with melt migration.

The presence of local dynamics visible in Figure 9 for models with melt migration makes these models significantly more dynamic and time-dependent than models without melt migration. Since melt affects both density, viscosity and temperature, the equations are coupled in a non-linear way, and these models require more computation time and are more sensitive to the chosen parameters. Furthermore, when melt migrates across the domain, its excess temperature and effect on further melting can cause a sort of positive feedback, resulting in increasing melt volumes and fractions being generated in a localized area; an effect that cannot be observed when calculating melt fractions as post-processing step. As a result of these local dynamics, both lithospheric thinning and magmatism will be more variable in time and space when melt migration is included. However, our models cannot simulate volcanism or dyke emplacement, since this would require even finer spatial and temporal resolution. Yet, including the local dynamics of melt seems to be necessary when modelling complex scenarios of plume-lithosphere interaction such as the emplacement of HALIP (compare Figures 1 and 2). While the assumption of melt being immediately extracted to the surface and not having any significant dynamic influence on mantle and lithosphere dynamics may be reasonable for settings with thin oceanic crust where melt can easily reach the surface, a thicker continental or cratonic lithosphere may require a more sophisticated approach that includes melt migration. A thick lithosphere can reduce the fraction of melt that can be extracted from the system, potentially even causing larger amounts of melt to pond beneath the lithosphere for a period of time (e.g., Aulbach et al., 2007, 2017; Sun et al., 2020). In this case, melt will have enough time to interact and affect local dynamics, which should therefore be taken into account when doing numerical models.

6 Discussion

Two of the main particularities of HALIP are the apparent extensive timing of emplacement (over 50 Myrs) and the documented pulses (e.g. earliest magmatism dating at 131 Ma, and pulses at 122, 95, 81 Ma Tegner et al., 2011; Dockman et al., 2018). These observations are in strong contrast to most other LIPs around the world, which are erupted within a very short time scale. As a consequence, there is an ongoing discussion as to whether HALIP is a large igneous province or not. Alternative explanations for at least part of the volcanism have been proposed, for example edge-driven convection north of the Greenland craton as the source for the secondary pulses (Dockman et al., 2018). Although edge-driven convection is known to be present at lithospheric steps (e.g., Manjón-Cabeza Córdoba & Ballmer, 2021, and references therein), it has been shown that the amount of melt being generated by this mechanism is small compared to plume-induced melting (Manjón-Cabeza Córdoba & Ballmer, 2021, 2022), and may only sustain small volcanic features such as seamounts. Another mechanism to generate melt in the presence of lithospheric steps is shear-driven upwelling (Conrad et al., 2010), but as for the edge-driven convection, expected melt volumes are small. So far, it has not been shown numerically, or otherwise, that edge-driven convection or shear-driven upwelling alone can produce melting as observed for HALIP. In contrast, our numerical models of a thermal mantle plume interacting with LAB topography dynamically produce rejuvenated magmatism with comparable timing and duration as has been observed for HALIP. While an extended suite of model runs with alternative parameter setups is beyond the scope

of this study, our results show that a mantle plume-related origin for many of the observed HALIP pulses is possible. Furthermore, HALIP magmatism shows compositions and characteristics of plume influence (e.g., Tegner et al., 2011; Buchan & Ernst, 2018; Bédard, Troll, et al., 2021; Senger & Galland, 2022). That said, depending on the paleotopography of the LAB, edge-driven convection or shear-driven upwelling (in addition to the convective patterns modelled here) may contribute to local dynamics and overall melt volumes and distributions (e.g., Conrad et al., 2010; Manjón-Cabeza Córdoba & Ballmer, 2022; Duvernay et al., 2022; Negredo et al., 2022).

Previous studies looking at melting in plumes have focused on different aspects of the problem, including melting in thermochemically zoned plumes (e.g., Dannberg & Gassmöller, 2018), melting in the presence of continental or cratonic lithosphere (Duvernay et al., 2022), or melting for specific plumes and tectonics settings (e.g., Ballmer et al., 2011; Bredow et al., 2017; Steinberger et al., 2019; Liu et al., 2021; Manjón-Cabeza Córdoba & Ballmer, 2022; Negredo et al., 2022). Even though the various model setups and levels of complexity are different, all studies of plume dynamics mentioned above have in common that they only consider simplified melt fractions, and do not model melt migration, as we do in this study. Some studies vary parameters related to melting changes such as the density (Ballmer et al., 2011; Bredow et al., 2017; Steinberger et al., 2019; Liu et al., 2021; Manjón-Cabeza Córdoba & Ballmer, 2022), viscosity (Ballmer et al., 2011; Bredow et al., 2017; Steinberger et al., 2019; Liu et al., 2021), or melting temperature (Ballmer et al., 2011; Negredo et al., 2022), and the work of Ballmer et al. (2011) on the Hawaiian Plume shows rejuvenated volcanism next to the plume track due to small-scale convection. While the the role of small-scale convection is important in both the work of Ballmer et al. (2011) and this study, the cases are not directly comparable. Hawaii is located far from any continent or craton on oceanic lithsphere older than ~ 70 Myr, which may have developed a washboard pattern of LAB topography before the plume hit the lithosphere (Ballmer et al., 2011). Rejuvenated melt is then generated by interaction of spreading plume material with this pre-existing pattern, but this is not applicable to the Arctic and HALIP. Furthermore, rejuvenated melting in Hawaii seems to happen within about 10 Myr, while HALIP volcanism is spread out over more than 30 Myr.

All of the studies given above assume that melt is immediately extracted from the model, and thus melt volumes are estimated as a post-processing step (Ballmer et al., 2011; Bredow et al., 2017; Steinberger et al., 2019). As a result, most of these studies show broad melting areas as we obtain for melt fractions in Figure 9 (top panels). This broad pattern contrasts the localized melting zones that evolve with melt migration (Figure 9 lower panels). Since most of previous studies look at plumes that impinge on oceanic lithosphere, it seems likely that most of the melt is quickly erupted, and thus the effect of excluding melt migration might be small. In contrast, continental or cratonic lithosphere may pose a barrier to rising melt, especially if the craton is intact (Aulbach et al., 2017). We have shown that if a significant portion of the melt will remain in the asthenosphere or lower lithosphere, it can be expected that the presence of melt significantly alters the local convection patterns (e.g. Figure 9). This feedback between melt and local dynamics is the cause of the rejuvenated magmatism we see in this study, and may explain the main difference between this work and the study of Duvernay et al. (2022), who report complex melting patterns in the presence of cratonic lithosphere, but do not observe rejuvenated volcanism. However, to capture plume-lithosphere dynamics correctly in settings with strong LAB topography, models need to include melt migration.

Despite the finding that our models can reproduce the prolonged melting and the pulses seen for HALIP, there are several assumptions and limitations that have to be taken into account. First of all, melt migration in ASPECT is modeled via Darcy's law, assuming that melt moves through the pore space of the ambient mantle or lithosphere. As a consequence, we cannot model melt eruptions, LIP emplacement or dyke intrusions, which are beyond the scope of this work. In fact, most of the melt in the models recrys-

tallizes close to the LAB instead of penetrating far into the lithosphere. Hence, our models may overestimate the impact of melting on lithosphere thinning. Furthermore, the amount of melt generated within the plume head is strongly dependent on parameters such as the surface solidus and the pressure gradient of the solidus. In addition, we only considered melting of dry peridotite, while the presence of water would facilitate more voluminous melting, or melting at lower temperatures or greater depths. In additon, our models are 2-D, and therefore cannot capture the full dynamics of plumes, which are 3-D features. However, models with melt migration are computationally expensive, making 3-D models difficult to realise. 2-D models also do not allow us to properly estimate melt volumes, which is the reason why we do not compare absolute melt volumes to estimates for HALIP. This problem is perhaps mitigated here because it is difficult reliably estimate melt volume for HALIP directly due to the large spatial spread of volcanism and difficulties to map intrusive and extrusive magmatism (Tegner et al., 2011; Senger & Galland, 2022). Furthermore, calculating time-integrated melt volumes from the porosity field alone is likely to underestimate the total melt volume of the model because melting / freezing and melt migration happen on timescales smaller than the timesteps at which the porosity field is updated.

Although modelled melt volumes cannot be compared to observations directly, it is obvious that the rejuvenated magmatism in our models is significantly smaller and more regionally confined than for the initial melting in the plume head (e.g. Figures 5a and 7b). For HALIP, it is extremely difficult to estimate the distribution and volumes of intrusive and extrusive magmatism, both for the initial phase and subsequent pulses (Figure 2). An areal estimate of 80,000 km^2 was proposed for the late-stage (85−60 Ma, third pulse) alkaline volcanism alone as defined by Tegner et al. (2011). More recently an accumulated magma volume of 100,000 km^3 was proposed by Saumur et al. (2016) for the Sverdrup Basin, without discriminating between the timing of this magmatism. Based on field mapping, Senger and Galland (2022) calculated 0.14−2.5 km^3 of emplaced magma in Svalbard alone, and expanding that to a regional (including Barents and Franz Josef Land) time-accumulated magma volume implies up to 200,000 km^3 based on geophysical data. These estimates do not include the ca. $1.3 \cdot 10^6$ km^2 areal extent of the Alpha Ridge Magmatic High (HAMH, Oakey and Saltus (2016); Figure 1), which would equal about $200 \cdot 10^6$ km^3 magma and therefore far exceed the continental (onshore or continental shelf) estimates listed above. Cumulative melt volumes for HALIP may therefore be in the order of $(200 - 300) \cdot 10^6$ km^3, but we lack clear constraints on the volumes of individual pulses. Hence, it seems plausible that the rejuvenated volcanism we see in our models can explain at least some of the locally confined alkalic magmatism observed for HALIP, but it is difficult to asses whether our model prediction of secondary pulses being about 2 orders of magnitude smaller than the initial pulse is realistic or not. Deviations between modeled and observed melt volumes may be partly explained by the difference between 2-D and 3-D geometry, which would allow for more local patches of melting and more realistic melt volumes. In addition, there are several potential mechanisms that could strengthen rejuvenated melting to produce a larger second pulse or even a third pulse of magmatism in the models. As geological data shows, the Arctic underwent extension at around the time of HALIP (e.g., Tegner et al., 2011). If melt-thinned areas are affected, this would enhance rejuvenated melting there. Distance and respective timing of the extension/ spreading would in this case determine the magnitude of melt generation, hence better constraints on plate reconstructions of the Arctic could be essential to explain HALIP. Another option to generate a more voluminous second pulse of melting could be a temporal variation in plume flux, which has been suggested for the Iceland plume based on V-shaped ridge segments in the North Atlantic (e.g., Ito, 2001; S. M. Jones et al., 2002; S. Jones et al., 2014; Parnell-Turner et al., 2014). Dynamically, such a plume pulse could be related to (potentially slab-driven) dynamics at the core-mantle boundary (e.g., Heyn et al., 2020), interaction with edge-driven convection (e.g., Manjón-Cabeza Córdoba & Ballmer, 2022; Negredo et al., 2022), solitary waves (Ito, 2001), or an interaction between the plume and the slab found underneath Green-

land at about 1000-1600 km depth (Shephard et al., 2016). Strong plume pulses or successful seafloor spreading can generate melting without the mechanism described in this paper, but a previously melt-influenced region of the lithosphere is more prone to rejuvenated melting, even without small changes in plume flux or failed rifting.

It is beyond the scope and capability of our models to predict compositions of generated melts, but our models show that the whole asthenosphere underneath the Sverdrup Basin region is influenced by the plume. As a consequence, we would expect that melting zones are plume-fed, with all of the generated melt having more or less plume-influenced compositions. However, the composition of melts is expected to change over time as the plume-lithosphere interaction evolves, and could also be influenced by pre-existing mantle chemistry - whether sub-continental or metasomatic mantle. Initial melts are likely to dominantly have the original (potentially deep-mantle) signature of the plume, which could shift towards enriched mantle (EM) signatures at later stages when more lower lithosphere is entrained in local convection cells where melt is generated. During the evolution of the system, further influences may come from pulses in plume flux, whether derived from the transition zone, lower mantle or plume-slab interactions. Finally, melt fractions and melting depths change significantly during the evolution of the system in our models (especially for the models accounting for melt migration). The first phase of melting in the the plume head is dominated by deep melts at lower melt fractions (that may never reach the surface), which rapidly changes towards predominantly shallower melting with large melt fractions. Over the next few million years, melt is generated at (locally increasingly) shallower depths, but melt fractions decrease until melting stops altogether. Rejuvenated melting is then characterized by low melt fractions at slightly deeper depths than the late stage of the first pulse. As a consequence, magmas can be expected to shift from mostly tholeiitic around the peak of the first pulse, to more alkalic at later stages of the first peak and in the second and third pulses. This trend seems to be supported by the data for HALIP (Figure 2). Models also indicate that the distribution of tholeiitic and alkalic magmatism may be not only time- but also location-dependent, and both types may be present at the same time, similar to what HALIP magmas suggest (Figure 2). However, in order to have a better constraint on the timing and locations of each magma type, we would need to add additional complexities to the model, e.g. run 3-D models and include more complex melting laws that track compositions in more detail. Future models could also address the broader HALIP geographic setting (Figure 1), beyond that of the Canadian Arctic Islands focused on here.

7 Conclusions

HALIP is an unusually large igneous province, if it is a LIP in the classic sense at all, because magmatism lasted for more than 50 Myr, with pulses of volcanic activity at around 122 Ma, 95 Ma and 81 Ma. So far, no conclusive mechanism has been proposed to explain this behaviour, since LIPs are typically emplaced within a short time, and edge-driven convection alone seems unlikely to explain the extent and volumes of magmatism in the Arctic, even for secondary pulses (Manjón-Cabeza Córdoba & Ballmer, 2021). In this work, we show that a mantle plume can produce prolonged melting periods and multiple events of melting in the same area if a plume interacts with tectonically inherited spatial variations in LAB depth, and if the lithosphere is locally thinned due small-scale convection associated with melt migrating upwards. More specifically, the plume head has to impinge on the thinner lithosphere of the basin, before the thicker continental margin and craton move over the plume stem. This variation in thickness channels plume flow in the asthenosphere towards the previously thinned lithosphere of the basin, where rejuvenated melting can occur. Considering the tectonic history of the Arctic and the presence of cratons around it, a non-uniform LAB thickness across the region seems plausible at the time of plume impingement. Hence, our models argue for a plume-related origin of most or even all the magmatism associated with HALIP. However, geodynamic

models investigating HALIP volcanism (and potentially other continental or cratonic LIPs) should include 2-phase flow melt migration to more accurately capture the dynamics affecting melt generation.

As shown by the numerical models, a plume head arriving underneath the extended lithosphere of the Sverdrup Basin would cause melting and further lithosphere thinning with strong local undulations in LAB depth, which can facilitate rejuvenated melting underneath the basin about 25-30 Myr later when the plume is underneath the Greenland craton and plume material is channeled towards the thinner basin. Melting depths and melt fractions vary throughout the time, and inferred compositions would be expected to change from more tholeiitic magmas for the first peak towards more alkalic magmas for later stages of the first peak and secondary pulses, but our models cannot track this in detail. While the simplified 2-D model used in this study can explain both timing and duration of the second pulse of melting for HALIP, relative melt volumes may not be representative for HALIP, and a third pulse cannot be reproduced. However, the magnitude of the second pulse of melting, and the presence and size of a potential third pulse, may be affected by contemporaneous tectonics (especially further extension or rifting), plume pulses generated at the core-mantle boundary, or plume-slab interaction related to the slab underneath Greenland (Shephard et al., 2016), all of which could easily reactivate or strengthen rejuvenated melting in areas that have been thinned by melt before. Finally, our models show that active melting does not necessarily happen above the plume, but lateral flow of plume may re-activate local melting in a previously plume-affected region up to a few hundred km away from the current plume position. Such complexity should be taken into account when using plume-related melting to infer plume positions, and when interpreting patterns of magmatism for HALIP and other LIPS or melting events close to continental or cratonic margins.

8 Open Research

Data presented in Figures 1 and 2, together with the ASPECT parameter files, ASPECT material model plugin, model data and postprocessing scripts used to generate and analyse the numerical models presented in this paper, are attached as zip folder for review and will be made available via Zenodo upon acceptance of the paper. ASPECT v2.4.0 (Bangerth et al., 2022) is freely available under the GPL v2.0 or later license, and can be accessed via https://geodynamics.org/resources/aspect or https://aspect.geodynamics.org, or via the github page https://github.com/geodynamics/aspect that includes the current development version of the code.

Acknowledgments

The authors acknowledge support from the Research Council of Norway through its Centers of Excellence funding scheme, Project Numbers 223272 and 332523, through the MAGPIE project, Project Number 288449, and through its Young Research Talent scheme for POLARIS - Evolution of the Arctic in Deep Time, Project Number 326238. Computations were made possible by the Norwegian Research Infrastructure Services (NRIS/sigma2) via allocations NN9283K, NS9029K and NN10003K. The authors declare no competing financial interests. We would like to thank the Computational Infrastructure for Geodynamics (geodynamics.org), which is funded by the National Science Foundation under award EAR-0949446 and EAR-1550901 for supporting the development of ASPECT.

References

Albers, M., & Christensen, U. R. (1996). The excess temperature of plumes rising from the core-mantle boundary. *Geophysical Research Letters*, *23*(24), 3567–3570. Retrieved from `https://agupubs.onlinelibrary.wiley.com/doi/abs/`

10.1029/96GL03311 doi: 10.1029/96GL03311

Aulbach, S., Griffin, W. L., Pearson, N. J., O'Reilly, S. Y., & Doyle, B. J. (2007). Lithosphere formation in the central slave craton (canada): plume subcretion or lithosphere accretion? *Contributions to Mineralogy and Petrology*, *154*(4), 409–427. doi: 10.1007/s00410-007-0200-1

Aulbach, S., Massuyeau, M., & Gaillard, F. (2017). Origins of cratonic mantle discontinuities: A view from petrology, geochemistry and thermodynamic models. *Lithos*, *268-271*, 364–382. Retrieved from http://www.sciencedirect.com/science/article/pii/S0024493716303905 doi: 10.1016/j.lithos.2016.11.004

Ballmer, M. D., Ito, G., van Hunen, J., & Tackley, P. J. (2011). Spatial and temporal variability in hawaiian hotspot volcanism induced by small-scale convection. *Nature Geoscience*, *4*(7), 457–460. doi: 10.1038/ngeo1187

Bangerth, W., Dannberg, J., Fraters, M., Gassmoeller, R., Glerum, A., Heister, T., ... Naliboff, J. (2022, July). *Aspect v2.4.0.* Zenodo. Retrieved from https://doi.org/10.5281/zenodo.6903424 doi: 10.5281/zenodo.6903424

Bédard, J. H., Saumur, B. M., Tegner, C., Troll, V. R., Deegan, F. M., Evenchick, C. A., ... Dewing, K. (2021, 06). Geochemical Systematics of High Arctic Large Igneous Province Continental Tholeiites from Canada—Evidence for Progressive Crustal Contamination in the Plumbing System. *Journal of Petrology*, *62*(9), egab041. Retrieved from https://doi.org/10.1093/petrology/egab041 doi: 10.1093/petrology/egab041

Bédard, J. H., Troll, V. R., Deegan, F. M., Tegner, C., Saumur, B. M., Evenchick, C. A., ... Dewing, K. (2021, 06). High Arctic Large Igneous Province Alkaline Rocks in Canada: Evidence for Multiple Mantle Components. *Journal of Petrology*, *62*(9), egab042. Retrieved from https://doi.org/10.1093/petrology/egab042 doi: 10.1093/petrology/egab042

Bredow, E., Steinberger, B., Gassmöller, R., & Dannberg, J. (2017). How plume-ridge interaction shapes the crustal thickness pattern of the réunion hotspot track. *Geochemistry, Geophysics, Geosystems*, *18*(8), 2930–2948. Retrieved from https://agupubs.onlinelibrary.wiley.com/doi/abs/10.1002/2017GC006875 doi: 10.1002/2017GC006875

Buchan, K. L., & Ernst, R. E. (2018). A giant circumferential dyke swarm associated with the high arctic large igneous province (halip). *Gondwana Research*, *58*, 39–57. Retrieved from https://www.sciencedirect.com/science/article/pii/S1342937X18300455 doi: 10.1016/j.gr.2018.02.006

Bédard, J. H., Troll, V. R., Deegan, F. M., Tegner, C., Saumur, B. M., Evenchick, C. A., ... Dewing, K. (2021, 06). High Arctic Large Igneous Province Alkaline Rocks in Canada: Evidence for Multiple Mantle Components. *Journal of Petrology*, *62*(9), egab042. Retrieved from https://doi.org/10.1093/petrology/egab042 doi: 10.1093/petrology/egab042

Coffin, M. F., & Eldholm, O. (1994). Large igneous provinces: Crustal structure, dimensions, and external consequences. *Reviews of Geophysics*, *32*(1), 1-36. Retrieved from https://agupubs.onlinelibrary.wiley.com/doi/abs/10.1029/93RG02508 doi: https://doi.org/10.1029/93RG02508

Conrad, C. P., Wu, B., Smith, E. I., Bianco, T. A., & Tibbetts, A. (2010). Shear-driven upwelling induced by lateral viscosity variations and asthenospheric shear: A mechanism for intraplate volcanism. *Physics of the Earth and Planetary Interiors*, *178*(3), 162–175. Retrieved from https://www.sciencedirect.com/science/article/pii/S003192010900209X doi: 10.1016/j.pepi.2009.10.001

Corfu, F., Polteau, S., Planke, S., Faleide, J. I., Svensen, H., Zayoncheck, A., & Stolbov, N. (2013, 06). U–Pb geochronology of Cretaceous magmatism on Svalbard and Franz Josef Land, Barents Sea Large Igneous Province. *Geological Magazine*, *150*(6), 1127-1135. Retrieved from https://doi.org/10.1017/

S0016756813000162 doi: 10.1017/S0016756813000162

Dannberg, J., & Gassmöller, R. (2018). Chemical trends in ocean islands explained by plume–slab interaction. *Proceedings of the National Academy of Sciences*, *115*(17), 4351–4356. Retrieved from https://www.pnas.org/content/115/17/4351 doi: 10.1073/pnas.1714125115

Dannberg, J., Gassmöller, R., Grove, R., & Heister, T. (2019, 05). A new formulation for coupled magma/mantle dynamics. *Geophysical Journal International*, *219*(1), 94–107. Retrieved from https://doi.org/10.1093/gji/ggz190 doi: 10.1093/gji/ggz190

Dannberg, J., & Heister, T. (2016). Compressible magma/mantle dynamics: 3D, adaptive simulations in ASPECT. *Geophysical Journal International*, *207*(3), 1343–1366. Retrieved from https://dx.doi.org/10.1093/gji/ggw329 doi: 10.1093/gji/ggw329

Dockman, D., Pearson, D., Heaman, L., Gibson, S., & Sarkar, C. (2018). Timing and origin of magmatism in the sverdrup basin, northern canada—implications for lithospheric evolution in the high arctic large igneous province (halip). *Tectonophysics*, *742-743*, 50–65. Retrieved from https://www.sciencedirect.com/science/article/pii/S004019511830180X doi: 10.1016/j.tecto.2018.05.010

Duvernay, T., Davies, D. R., Mathews, C. R., Gibson, A. H., & Kramer, S. C. (2022). Continental magmatism: The surface manifestation of dynamic interactions between cratonic lithosphere, mantle plumes and edge-driven convection. *Geochemistry, Geophysics, Geosystems*, *23*(7), e2022GC010363. Retrieved from https://agupubs.onlinelibrary.wiley.com/doi/abs/10.1029/2022GC010363 (e2022GC010363 2022GC010363) doi: 10.1029/2022GC010363

Døssing, A., Gaina, C., & Brozena, J. M. (2017). Building and breaking a large igneous province: An example from the high arctic. *Geophysical Research Letters*, *44*(12), 6011-6019. Retrieved from https://agupubs.onlinelibrary.wiley.com/doi/abs/10.1002/2016GL072420 doi: https://doi.org/10.1002/2016GL072420

Estrada, S. (2015). Geochemical and sr–nd isotope variations within cretaceous continental flood-basalt suites of the canadian high arctic, with a focus on the hassel formation basalts of northeast ellesmere island. *International Journal of Earth Sciences*, *104*, 1981-2005. doi: https://doi.org/10.1007/s00531-014-1066-x

Estrada, S., Damaske, D., Henjes-Kunst, F., Schreckenberger, B., Oakey, G. N., Piepjohn, K., ... Linnemann, U. (2016). Multistage cretaceous magmatism in the northern coastal region of ellesmere island and its relation to the formation of alpha ridge - evidence from aeromagnetic, geochemical and geochronological data. *Norwegian Journal of Geology*, *96*(2). doi: 10.17850/njg96-2-03

Estrada, S., & Henjes-Kunst, F. (2004). Volcanism in the canadian high arctic related to the opening of the arctic ocean. *Zeitschrift der Deutschen Geologischen Gesellschaft*, *154*, 579-603. doi: 10.1127/zdgg/154/2004/579

Estrada, S., Henjes-Kunst, F., Melcher, F., & Tessensohn, F. (2010). Paleocene alkaline volcanism in the nares strait region: evidence from volcanic pebbles. *International Journal of Earth Sciences*, *99*. doi: 10.1007/s00531-009-0432-6

Evenchick, C. A., Davis, W. J., Bédard, J. H., Hayward, N., & Friedman, R. M. (2015, 09). Evidence for protracted High Arctic large igneous province magmatism in the central Sverdrup Basin from stratigraphy, geochronology, and paleodepths of saucer-shaped sills. *GSA Bulletin*, *127*(9-10), 1366-1390. Retrieved from https://doi.org/10.1130/B31190.1 doi: 10.1130/B31190.1

Galloway, J. M., Fensome, R. A., Swindles, G. T., Hadlari, T., Fath, J., Schröder-Adams, C., ... Pugh, A. (2022). Exploring the role of high arctic large igneous province volcanism on early cretaceous arctic forests. *Cretaceous*

Research, *129*, 105022. Retrieved from https://www.sciencedirect.com/science/article/pii/S0195667121002706 doi: https://doi.org/10.1016/j.cretres.2021.105022

Hadlari, T., Dewing, K., Matthews, W. A., Alonso-Torres, D., & Midwinter, D. (2018). Early triassic development of a foreland basin in the canadian high arctic: Implications for a pangean rim of fire. *Tectonophysics*, *736*, 75-84. Retrieved from https://www.sciencedirect.com/science/article/pii/S004019511830163X doi: https://doi.org/10.1016/j.tecto.2018.04.020

Heister, T., Dannberg, J., Gassmöller, R., & Bangerth, W. (2017). High accuracy mantle convection simulation through modern numerical methods. II: Realistic models and problems. *Geophysical Journal International*, *210*(2), 833–851. Retrieved from https://doi.org/10.1093/gji/ggx195 doi: 10.1093/gji/ggx195

Heyn, B. H., & Conrad, C. P. (2022). On the relation between basal erosion of the lithosphere and surface heat flux for continental plume tracks. *Geophysical Research Letters*, *49*(7), e2022GL098003. Retrieved from https://agupubs.onlinelibrary.wiley.com/doi/abs/10.1029/2022GL098003 (e2022GL098003 2022GL098003) doi: 10.1029/2022GL098003

Heyn, B. H., Conrad, C. P., & Trønnes, R. G. (2020). How thermochemical piles can (periodically) generate plumes at their edges. *Journal of Geophysical Research: Solid Earth*, *125*(6), e2019JB018726. Retrieved from https://agupubs.onlinelibrary.wiley.com/doi/abs/10.1029/2019JB018726 (e2019JB018726 10.1029/2019JB018726) doi: 10.1029/2019JB018726

Ito, G. (2001). Reykjanes 'v'-shaped ridges originating from a pulsing and dehydrating mantle plume. *Nature*, *411*(6838), 681–684. doi: 10.1038/35079561

Jackson, H. R., Dahl-Jensen, T., & working group, L. (2010, 07). Sedimentary and crustal structure from the Ellesmere Island and Greenland continental shelves onto the Lomonosov Ridge, Arctic Ocean. *Geophysical Journal International*, *182*(1), 11–35.

Jakobsson, M., Mayer, L., Coakley, B., Dowdeswell, J. A., Forbes, S., Fridman, B., ... Weatherall, P. (2012). The international bathymetric chart of the arctic ocean (ibcao) version 3.0. *Geophysical Research Letters*, *39*(12). Retrieved from https://agupubs.onlinelibrary.wiley.com/doi/abs/10.1029/2012GL052219 doi: 10.1029/2012GL052219

Jokat, W., Ickrath, M., & O'Connor, J. (2013). Seismic transect across the lomonosov and mendeleev ridges: Constraints on the geological evolution of the amerasia basin, arctic ocean. *Geophysical Research Letters*, *40*(19), 5047-5051. Retrieved from https://agupubs.onlinelibrary.wiley.com/doi/abs/10.1002/grl.50975 doi: https://doi.org/10.1002/grl.50975

Jones, S., Murton, B., Fitton, J., White, N., Maclennan, J., & Walters, R. (2014). A joint geochemical–geophysical record of time-dependent mantle convection south of iceland. *Earth and Planetary Science Letters*, *386*, 86–97. Retrieved from http://www.sciencedirect.com/science/article/pii/S0012821X13005402 doi: 10.1016/j.epsl.2013.09.029

Jones, S. M., White, N., & Maclennan, J. (2002). V-shaped ridges around iceland: Implications for spatial and temporal patterns of mantle convection. *Geochemistry, Geopysics, Geosystems*, *3*(10), 1059. Retrieved from https://agupubs.onlinelibrary.wiley.com/doi/10.1029/2002GC000361 doi: 10.1029/2002GC000361

Jowitt, S. M., Williamson, M.-C., & Ernst, R. E. (2014, 03). Geochemistry of the 130 to 80 Ma Canadian High Arctic Large Igneous Province (HALIP) Event and Implications for Ni-Cu-PGE Prospectivity. *Economic Geology*, *109*(2), 281–307. Retrieved from https://doi.org/10.2113/econgeo.109.2.281 doi: 10.2113/econgeo.109.2.281

Kontak, D. J., Jensen, S. M., Dostal, J., Archibald, D. A., & Kyser, T. K. (2001,

08). CRETACEOUS MAFIC DYKE SWARM, PEARY LAND, NORTHERNMOST GREENLAND: GEOCHRONOLOGY AND PETROLOGY. *The Canadian Mineralogist*, *39*(4), 997-1020. Retrieved from https://doi.org/10.2113/gscanmin.39.4.997 doi: 10.2113/gscanmin.39.4.997

Kronbichler, M., Heister, T., & Bangerth, W. (2012). High accuracy mantle convection simulation through modern numerical methods. *Geophysical Journal International*, *191*, 12–29. Retrieved from http://dx.doi.org/10.1111/j.1365-246X.2012.05609.x doi: 10.1111/j.1365-246X.2012.05609.x

Lawver, L. A., & Müller, R. D. (1994, 04). Iceland hotspot track. *Geology*, *22*(4), 311–314. Retrieved from https://doi.org/10.1130/0091-7613(1994)022<0311:IHT>2.3.CO;2 doi: 10.1130/0091-7613(1994)022⟨0311:IHT⟩2.3.CO;2

Lebedeva-Ivanova, N., Gaina, C., Minakov, A., & Kashubin, S. (2019). Arccrust: Arctic crustal thickness from 3-d gravity inversion. *Geochemistry, Geophysics, Geosystems*, *20*(7), 3225-3247. Retrieved from https://agupubs.onlinelibrary.wiley.com/doi/abs/10.1029/2018GC008098 doi: https://doi.org/10.1029/2018GC008098

Liu, J., Pearson, D. G., Wang, L. H., Mather, K. A., Kjarsgaard, B. A., Schaeffer, A. J., ... Armstrong, J. P. (2021). Plume-driven recratonization of deep continental lithospheric mantle. *Nature*, *592*(7856), 732–736. doi: 10.1038/s41586-021-03395-5

Maher, H. D., Jr. (2001). Manifestations of the cretaceous high arctic large igneous province in svalbard. *The Journal of Geology*, *109*(1), 91-104. doi: 10.1086/317960

Manjón-Cabeza Córdoba, A., & Ballmer, M. D. (2021). The role of edge-driven convection in the generation of volcanism – part 1: A 2d systematic study. *Solid Earth*, *12*(3), 613–632. Retrieved from https://se.copernicus.org/articles/12/613/2021/ doi: 10.5194/se-12-613-2021

Manjón-Cabeza Córdoba, A., & Ballmer, M. D. (2022). The role of edge-driven convection in the generation of volcanism – part 2: Interaction with mantle plumes, applied to the canary islands. *Solid Earth*, *13*(10), 1585–1605. Retrieved from https://se.copernicus.org/articles/13/1585/2022/ doi: 10.5194/se-13-1585-2022

Martos, Y. M., Jordan, T. A., Catalán, M., Jordan, T. M., Bamber, J. L., & Vaughan, D. G. (2018). Geothermal heat flux reveals the iceland hotspot track underneath greenland. *Geophysical Research Letters*, *45*(16), 8214–8222. Retrieved from https://agupubs.onlinelibrary.wiley.com/doi/abs/10.1029/2018GL078289 doi: 10.1029/2018GL078289

Midtkandal, I., Faleide, J. I., Faleide, T. S., Serck, C. S., Planke, S., Corseri, R., ... Nystuen, J. P. (2020). Lower cretaceous barents sea strata: epicontinental basin configuration, timing, correlation and depositional dynamics. *Geological Magazine*, *157*(3), 458–476. doi: 10.1017/S0016756819000918

Minakov, A., Yarushina, V., Faleide, J. I., Krupnova, N., Sakoulina, T., Dergunov, N., & Glebovsky, V. (2018). Dyke emplacement and crustal structure within a continental large igneous province, northern barents sea. *Geological Society, London, Special Publications*, *460*(1), 371–395. Retrieved from https://www.lyellcollection.org/doi/abs/10.1144/SP460.4 doi: 10.1144/SP460.4

Naber, T., Grasby, S., Cuthbertson, J., Rayner, N., & Tegner, C. (2020, 12). New constraints on the age, geochemistry, and environmental impact of High Arctic Large Igneous Province magmatism: Tracing the extension of the Alpha Ridge onto Ellesmere Island, Canada. *GSA Bulletin*, *133*(7-8), 1695–1711. Retrieved from https://doi.org/10.1130/B35792.1 doi: 10.1130/B35792.1

Negredo, A. M., van Hunen, J., Rodríguez-González, J., & Fullea, J. (2022). On the origin of the canary islands: Insights from mantle convection modelling.

Earth and Planetary Science Letters, *584*, 117506. Retrieved from https://www.sciencedirect.com/science/article/pii/S0012821X2200142X doi: 10.1016/j.epsl.2022.117506

Oakey, G., & Saltus, R. (2016). Geophysical analysis of the alpha–mendeleev ridge complex: Characterization of the high arctic large igneous province. *Tectonophysics*, *691*, 65-84. Retrieved from https://www.sciencedirect.com/science/article/pii/S0040195116303304 (SI:Circum-Arctic Evolution) doi: https://doi.org/10.1016/j.tecto.2016.08.005

Parnell-Turner, R., White, N., Henstock, T., Murton, B., Maclennan, J., & Jones, S. M. (2014). A continuous 55-million-year record of transient mantle plume activity beneath iceland. *Nature Geoscience*, *7*(12), 914–919. doi: 10.1038/ngeo2281

Pease, V., Drachev, S., Stephenson, R., & Zhang, X. (2014). Arctic lithosphere — a review. *Tectonophysics*, *628*, 1-25. Retrieved from https://www.sciencedirect.com/science/article/pii/S0040195114003060 doi: https://doi.org/10.1016/j.tecto.2014.05.033

Polteau, S., Hendriks, B. W., Planke, S., Ganerød, M., Corfu, F., Faleide, J. I., ... Myklebust, R. (2016). The early cretaceous barents sea sill complex: Distribution, 40ar/39ar geochronology, and implications for carbon gas formation. *Palaeogeography, Palaeoclimatology, Palaeoecology*, *441*, 83–95. Retrieved from https://www.sciencedirect.com/science/article/pii/S0031018215003673 (Impact, Volcanism, Global changes and Mass Extinctions) doi: 10.1016/j.palaeo.2015.07.007

Saumur, B., Dewing, K., & Williamson, M.-C. (2016). Architecture of the canadian portion of the high arctic large igneous province and implications for magmatic ni–cu potential. *Canadian Journal of Earth Sciences*, *53*(5), 528-542. doi: 10.1139/cjes-2015-0220

Schaeffer, A. J., & Lebedev, S. (2013, 04). Global shear speed structure of the upper mantle and transition zone. *Geophysical Journal International*, *194*(1), 417-449. Retrieved from https://doi.org/10.1093/gji/ggt095 doi: 10.1093/gji/ggt095

Senger, K., & Galland, O. (2022). Stratigraphic and spatial extent of halip magmatism in central spitsbergen. *Geochemistry, Geophysics, Geosystems*, *23*(11), e2021GC010300. Retrieved from https://agupubs.onlinelibrary.wiley.com/doi/abs/10.1029/2021GC010300 (e2021GC010300 2021GC010300) doi: 10.1029/2021GC010300

Shephard, G. E., Müller, R. D., & Seton, M. (2013, September). The tectonic evolution of the Arctic since Pangea breakup: Integrating constraints from surface geology and geophysics with mantle structure. *Earth-Science Reviews*, *124*, 148–183. Retrieved 2022-10-17, from https://linkinghub.elsevier.com/retrieve/pii/S0012825213001104 doi: 10.1016/j.earscirev.2013.05.012

Shephard, G. E., Trønnes, R. G., Spakman, W., Panet, I., & Gaina, C. (2016). Evidence for slab material under greenland and links to cretaceous high arctic magmatism. *Geophysical Research Letters*, *43*(8), 3717–3726. Retrieved from https://agupubs.onlinelibrary.wiley.com/doi/abs/10.1002/2016GL068424 doi: 10.1002/2016GL068424

Steffen, R., Audet, P., & Lund, B. (2018). Weakened lithosphere beneath greenland inferred from effective elastic thickness: A hot spot effect? *Geophysical Research Letters*, *45*(10), 4733-4742. Retrieved from https://agupubs.onlinelibrary.wiley.com/doi/abs/10.1029/2017GL076885 doi: https://doi.org/10.1029/2017GL076885

Steinberger, B., Bredow, E., Lebedev, S., Schaeffer, A., & Torsvik, T. H. (2019). Widespread volcanism in the greenland–north atlantic region explained by the iceland plume. *Nature Geoscience*, *12*(1), 61–68. doi: 10.1038/s41561-018-0251-0;10.1038/s41561-018-0251-0

Sun, P., Niu, Y., Guo, P., Duan, M., Wang, X., Gong, H., & Xiao, Y. (2020). The lithospheric thickness control on the compositional variation of continental intraplate basalts: A demonstration using the cenozoic basalts and clinopyroxene megacrysts from eastern china. *Journal of Geophysical Research: Solid Earth*, *125*(3), e2019JB019315. Retrieved from `https://agupubs.onlinelibrary.wiley.com/doi/abs/10.1029/2019JB019315` (e2019JB019315 2019JB019315) doi: 10.1029/2019JB019315

Tarduno, J. (1998). The high arctic large igneous province. *Third International Conference on Arctic margins [ICAM III], Celle, Germany, Fed. Inst. Geosci. Nat Res. Abstract.*.

Tegner, C., Storey, M., Holm, P., Thorarinsson, S., Zhao, X., Lo, C.-H., & Knudsen, M. (2011). Magmatism and eurekan deformation in the high arctic large igneous province: 40ar–39ar age of kap washington group volcanics, north greenland. *Earth and Planetary Science Letters*, *303*(3), 203–214. Retrieved from `https://www.sciencedirect.com/science/article/pii/S0012821X10008204` doi: 10.1016/j.epsl.2010.12.047

Thorarinsson, S. B., Holm, P. M., Tappe, S., Heaman, L. M., & Tegner, C. (2011). Late cretaceous–palaeocene continental rifting in the high arctic: U–pb geochronology of the kap washington group volcanic sequence, north greenland. *Journal of the Geological Society*, *168*(5), 1093-1106. Retrieved from `https://www.lyellcollection.org/doi/abs/10.1144/0016-76492011-018` doi: 10.1144/0016-76492011-018

Trettin, H. E. (n.d.). Geology of canada, no. 3; geology of the innuitian orogen and arctic platform of canada and greenland.(569 pp.). *Geological Survey of Canada*(3).

Villeneuve, M., & Williamson, M.-C. (2006). 40Ar-39Ar dating of mafic magmatism from the Sverdrup Basin Magmatic Province. *Scott, R.A., Thurston, D.K. (Eds.), ICAM IV Proceedings, Dartmouth, Nova Scotia*, 206-215.